Chem Soc Rev

REVIEW ARTICLE

Chemical designs of functional photoactive molecular assemblies

Cite this: DOI: 10.1039/c3cs60375j

Qifan Yan, Zhouyang Luo, Kang Cai, Yuguo Ma* and Dahui Zhao*

Received 22nd October 2013

DOI: 10.1039/c3cs60375j

www.rsc.org/csr

Molecular assemblies with well-defined structures capable of photo-induced electron transfer and charge transport or photochemical reactions are reviewed. Hierarchical supramolecular architectures, which assemble the modular units into specific spatial arrangements and facilitate them to work cooperatively, are vital for the achievement of photo-functions in these systems. The chemical design of molecular building blocks and noncovalent interactions exploited to realize supramolecular organizations are particularly discussed. Reviewing and recapitulating the chemical evolution traces of these accomplished systems will hopefully delineate certain fundamental design principles and guidelines useful for developing more advanced functions in the future.

1 Introduction

Molecules in an aggregated state may exhibit distinct photochemical behaviors from those of single molecules.[1] An eminent example is the natural photosynthetic system, in which chlorophyll dyes are assembled in an ordered fashion to promote efficient light harvesting and redox reactions.[2,3] Inspired by this perfect paradigm, scientists have endeavored to create molecular systems which can collect solar energy and effectively transform it into chemical, electric, or other forms of energy.[4–17] Although we are still on the way toward attaining advanced functional systems, it has been realized that rational design of hierarchical architectures is crucial to achieving complex functions. Moreover, as demonstrated by the natural photosynthetic system, in addition to covalent bonds, noncovalent interactions are valuable tools for constructing hierarchical structures with molecular building blocks, as they allow for more facile and versatile assembling tactics.

We herein review a number of recently reported supramolecular assemblies which are designed to perform photochemical functions. Photo-induced electron transfer and photochemical reactions are two types of functions that attract many research efforts.[18,19] In the former case, charge-separated states are

Beijing National Laboratory for Molecular Sciences, Key Laboratory of Polymer Chemistry and Physics of the Ministry of Education, College of Chemistry, Peking University, China

Qifan Yan

Dr Qifan Yan was born in China in 1984. He obtained a Bachelor of Science degree at Peking University in 2007, and then began his graduate study at the same university. In 2012, he obtained his PhD in chemistry researching and studying the synthesis and photophysical properties of conjugated oligomers, under the supervision of Prof. Dahui Zhao. After a year's postdoctoral work at Prof. Yuguo Ma's group working on solid-state reactions under high pressure, he has now joined Prof. Eiichi Nakamura's group as a postdoc fellow at the University of Tokyo in Japan.

Zhouyang Luo

Zhouyang Luo was born in China in 1989. He obtained a Bachelor of Science degree at Peking University in 2011, and then began his graduate study at the same university under the supervision of Prof. Dahui Zhao. His research interests mainly focus on studying conjugated foldamers and syntheses of large polycyclic π-conjugated molecules.

further stabilized by delocalization of holes and/or electrons among aggregated monomers. Furthermore, by virtue of long-range orbital coupling, charge carrier transport may be realized in the aggregates. For photochemical transformations, the defined intermolecular arrangements conferred by aggregation may enable better or different regio- or stereo-selectivities than those observed in a molecularly dissolved state.[20–24] Evidently, the realization of such functions relies on both the chemical characters of the assembly building blocks and the intermolecular organization motifs, the latter of which governs the spatial arrangements of molecules. Only when appropriate organizations are achieved, could the molecules work cooperatively in the desired fashion. To achieve such challenging tasks, rational designs are warranted.[25–27] The focus of design is the chemical identities of the monomers, as they lend the basis to both supramolecular associations and photochemical functions. The following examples illustrate such sensible design tactics. By chemically tailoring the building block structures, researchers create, adapt, and tweak the assembly structures to eventually realize or improve the functional performance.

In the first part of this article, molecular assemblies capable of photo-induced electron-transfer are reviewed. In the second part, examples of photochemical transformations that uniquely take place in molecular aggregates and are influenced by supramolecular structures are discussed. As we herein set a main focus on the intermolecular interactions and their influence over photochemical reactions, those transformations that are not unique to molecular aggregates but similarly happen with single molecules, such as the isomerization of azabenzene and diarylethene,[28–31] are not included. Both sections are organized around intermolecular interactions which are employed to construct and stabilize the photoactive assemblies. Particular emphases are laid on the chemical structures readily offering such interactions, as well as the characteristics of supramolecular scaffolds constructed to fulfill the photo-induced functions.

The scope of this contribution is limited to molecular assemblies that manifest photochemical functions. A range of molecular aggregates showing photophysical activities reported in the literature are not covered, since a number of previous reviews have nicely summarized the relevant work.[32–36] Examples of interesting photophysical processes manifested by such molecular aggregates include FRET (Förster resonant energy transfer), triplet exciton generation *via* singlet fission, fluorescence sensing, aggregation induced emission, *J*-aggregation, *etc.* It should be noted that the formation of supramolecular architectures is dictated by the intermolecular interactions among the composing building blocks (monomers), along with their interactions with the environment (*e.g.* solvents). These molecular interactions are intrinsically encoded in the chemical structures of the monomers, disregarding whether photochemical or photophysical processes would ensue.

Kang Cai

Kang Cai was born in China in 1988. He received his BS degree from Peking University in 2011. He is now a graduate student under the supervision of Prof. Dahui Zhao. His research is currently focused on the development of novel heteroacene dicarboximides for organic semiconductors and functional molecular assemblies.

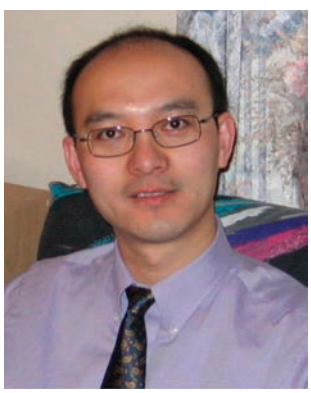

Yuguo Ma

Prof. Yuguo Ma, born in 1972, obtained his BSc (Hons) in 1994 and MSc in 1997 from College of Chemistry at Peking University under supervision of Prof. Qi-Feng Zhou. He continued his graduate study at University of Illinois at Urbana-Champaign with Prof. Steven C. Zimmerman obtaining his PhD in 2002. From 2003 to 2005, he was a postdoc research associate with Prof. Geoffrey W. Coates at Cornell University. In September 2005, he returned to Peking University as an associate professor of chemistry, and promoted to full Professor in 2011. His current research interests include supramolecular chemistry, self-assembly & molecular recognition, and organic/polymer functional materials.

Dahui Zhao

Prof. Dahui Zhao was born in China, 1974. She received her BS from Peking University in 1997, and PhD in chemistry from University of Illinois at Urbana-Champaign in 2003 with Prof. Jeffrey Moore. After working with Prof. Timothy Swager at MIT as a postdoc associate, she returned to Peking University in 2006 and is now an associate professor. Her main research interests include designing and studying large polycyclic molecules and oligomers of conjugated structures.

Therefore, the design principles and strategies for creating supramolecular identities illustrated by the following systems are equally applicable to photophysical processes. Nonetheless, photochemical processes often impose more rigorous constraints on the supramolecular platforms. For example, vital conditions for realizing photo-induced electron transfer and charge transport include suitable spatial distances between donor and acceptor groups, appropriate phase separation patterns, *etc.* Similarly, only when very particular molecular arrangements and functional group orientations are provided, can photochemical reactions happen within molecular aggregates. In view of such complexities, meticulous thought ought to be given to designing supramolecular assemblies capable of accomplishing photochemical functions. By bringing together a number of pertinent, representative examples featuring elegant rational designs, the current review hopes to offer certain useful information, facilitating the future work in this field.

Moreover, the following discussion is mostly focused on aggregate structures that can be stabilized in nanometer dimensions in solvent media. The large volume of literature reporting on photochemical processes taking place in the solid (crystalline) state are not extensively included.[23,24,37,38] Also, most of the work reviewed herein concerns supramolecular assemblies with well-defined structures. Aggregates with disordered structures or ill-defined molecular arrangements are not particularly introduced, as they usually provide unreliable information on the supramolecular interactions and structures.

2 Photo-induced electron transfer and charge transport in molecular assemblies

Photo-induced electron transfer and charge transport processes are of paramount importance, because they constitute the basis for organic photovoltaics. The occurrence of photo-induced electron transfer typically relies on coupling an electron donor with an acceptor having suitable frontier molecular orbitals. In terms of chemical structures, frequently employed donor groups in the literature are electron-rich conjugated structures, including porphyrins, polycyclic aromatics, and so on. Fullerene and electron-deficient aromatic molecules, *e.g.*, perylene and naphthalene diimide derivatives, are often used as electron acceptors.

Segregated associations of donor and acceptor groups help to enhance the efficiency of electron transfer by spatially separating the hole and electron, and more effectively by stabilizing the carriers *via* charge delocalization.[39–41] More importantly, when proper aggregate structures are provided, *e.g.*, suitably face-to-face stacked aromatic moieties, continuous paths for transporting charge carriers can be formed. In certain systems, segregated donor–acceptor domains comprising molecules packed in an ordered fashion may grow up to nano-scale sizes. Upon photo-excitation, a photo-current can then be generated where the holes and electrons are transported continuously in separate channels. Given suitable conditions, a hetero-junction photovoltaic device may thus be realized. Therefore, the suitable supramolecular organization of donors and acceptors is a key factors in accomplishing the above processes.[42–47] Certain aggregation motifs, like an alternating donor–acceptor arrangement, which disfavors charge separation and transport, should be avoided.

In the following discussion, particular attention is paid to various noncovalent interactions harnessed for constructing different supramolecular assemblies. Although noncovalent forces (2–300 kJ mol^{-1}) are typically weaker than covalent bonds, the collective strengths among numerous assembled monomers sufficiently afford stable aggregate structures. The unique merits of such noncovalent interactions are their reversibility and facile formation under ambient conditions. These properties are quite valuable for building complex hierarchical systems, as they allow for the convenient application of a self-assembly approach.[1,48]

The availability of diverse noncovalent forces underlies the versatility and potency of the self-assembly strategy, although each type of bond may have its own pros and cons. For example, metal–ligand coordination is a relatively robust and highly directional noncovalent interaction, but its occurrence relies on the presence of very specific functional groups in the substrates. On the other hand, π–π interactions widely exist with various aromatic molecules. Nowadays, benefitting from the development of organic electronics and optics, a range of π-conjugated structures possessing optimal light absorbability and suitable frontier orbitals have been prepared and studied for photoconducting and photovoltaic applications in the bulk phase. Thus, a large number of chemical structures capable of aromatic stacking interactions are available as potential building blocks for designing photoactive assemblies. In addition to its ubiquitous occurrence, another unparalleled advantage of π–π interactions is that charge transport channels are potentially formed by appropriately stacked aromatic molecules.[49,50] Hydrogen bonding is another type of commonly employed noncovalent force, with ready availability and tunable strength from a variety of chemical functionalities.[51,52] This noncovalent bond has a certain directionality, but is less stringent compared to the metal–ligand interaction. Furthermore, combining different types of noncovalent interactions and promoting them to work cooperatively offers a powerful approach to build complex supramolecular assemblies for accomplishing sophisticated functions.

In the following sections, a number of molecular assemblies capable of photo-induced electron-transfer are reviewed, categorized by the type of noncovalent forces mainly responsible for driving the assembly formation. Table 1 summarizes the important features of the reviewed systems in this part.

2.1 Molecular assemblies with metal–ligand interactions

The metal–ligand coordination interaction is a robust and directional noncovalent force. The directionality is determined by the coordination geometries. These features make coordination a somewhat special type of interaction, dissimilar to other

Table 1 Assembly properties and photoactivities of molecular aggregates

Compound	Major driving force[a]	Aggregate-forming conditions[b]	Photoactivity[c]	Ref.
D(ZnP)$_n$ –C60py	M–L	Dissolving	CS	60
Rail–Rung1	M–L	Dissolving	CS	61
HBC-3	π–π & solvophobic	Mixed solvents	I_{ph}	66–68
HBC-4		Cooling	PV	
HBC-1– HBC-4		Cooling	PV	
HBC-5		Dissolving	TRMC	
Th–C60-1	π–π	LC phase	I_{ph} & TRMC	69
(+)- **Por–C60-1**	π–π & solvophobic	Mixed solvents	I_{ph} & TOF	70
ZnP–C60-1	π–π & solvophobic	Mixed solvents	PV	72
Th–PDI-1	π–π & solvophobic	Cooling	I_{ph}	73
NDI–Por2	π–π, H-bond & solvophobic	Dissolving	CS	81
OPV:PDI	π–π, H-bond & solvophobic	Cooling or evaporating	CS	82 and 83
ZnCh3	M–L, H-bond, π–π & solvophobic	Mixed solvents	TRMC	88
Ph-NDI1–3	Electrostatic, H-bond & π–π	Layer-by-layer	I_{ph}	92
Au–(**Ph-NDIX**)$_n$–			PV	93
Au–(**OPE-NDIX**)$_n$–			I_{ph}	95
ITO–(NDIX)$_n$–	Electrostatic, H-bond & π–π	SOSIP	I_{ph}	96
SOSIP–PDI1–2			PV & I_{ph}	97
NDI–Sq-C60			I_{ph}	100

[a] M–L, metal–ligand coordination; π–π, aromatic stacking; solvophobic, hydrophobic interactions with polar solvents and/or lipophilic interactions among alkyl chains. [b] Dissolving, dissolving molecules in suitable solvents; mixed solvents, slowly adding or diffusing a poor solvent to a solution of good solvent; cooling, slowly cooling a hot solution; evaporating, slowly evaporating solvent molecules. [c] CS, charge separation; I_{ph}, photocurrent; PV, photovoltaic response; TRMC, time-resolved microwave conductivity; TOF, time-of-flight mobility measurement.

noncovalent forces. It is thus uniquely useful in building supramolecular assemblies.

As it is applied in natural light harvesting chlorophyll arrays, the coordination bond is often employed to develop photoactive molecular assemblies with biomimetic characters, namely as photosynthetic mimicry.[53,54] Relevant systems often recruit porphyrins or phthalocyanines as building blocks, since they have an intrinsic coordination cavity for accommodating metal ions. As electron donors, porphyrins and phthalocyanines may work in conjugation with electron acceptors, *e.g.*, fullerene.[55] In the literature, N-heterocycles such as pyridine and imidazole are covalently tethered to fullerenes,[56–58] and upon coordinating to a metalloporphyrin or phthalocyanine, spatial proximity is achieved between the fullerene and donor group, giving rise to electron transfer under light illumination. The association constants of metalloporphyrins with fullerene are typically tens of thousands per mole. Single crystal analysis verified the structure of a 1 : 1 complex of fullerene with zinc porphyrin.[56] It should be noted that in the presence of solvent molecules with competing coordination abilities, the acceptor ligand may be replaced, resulting in disruption of the desired complexes.[56–58]

In order to attain larger supramolecular assemblies composed of such metal–ligand interactions, one possible method is to prepare bis-functionalized molecules. However, when two pyridine units were ligated to a fullerene molecule, and two porphyrin groups were covalently joined into a dimer, a 1 : 1 complex instead of a supramolecular polymer still resulted, with both zinc-porphyrins from the dimer coordinated to the two pyridines from the same fullerene.[59] A larger association constant was determined for such a doubly complexed triad, and photo-induced electron transfer was confirmed to occur within this cyclic structure by transient absorption characterizations (Chart 1).

An alternative approach was taken by Fukuzumi *et al.* to create large, coordinated supramolecular assemblies with zinc-porphyrin and fullerene partners. A series of PAMAM dendrimers up to three generations were prepared, which were decorated with 4, 8, or 16 zinc porphyrins at peripheral positions.[60] A corresponding number of pyridine ligands bearing fulleropyrrolidine was then coordinated to these zinc porphyrin units as electron acceptors (Chart 2). Resulting from a dendritic effect, highly efficient exciton migration occurred among the porphyrin units in **D(ZnP)$_{16}$** before electron transfer to the C_{60} moiety happened. A particularly long lifetime was detected for the charge-separated state of this dendritic supramolecular assembly, which presumably was related to the charge (hole and/or electron) delocalization among the multiple donors and/or acceptors in this dendrimer complex.

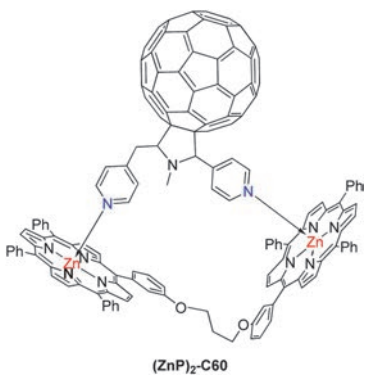

Chart 1 Chemical structure of a 1 : 1 complex of bipyridine-substituted fullerene with a porphyrin dimer.[59]

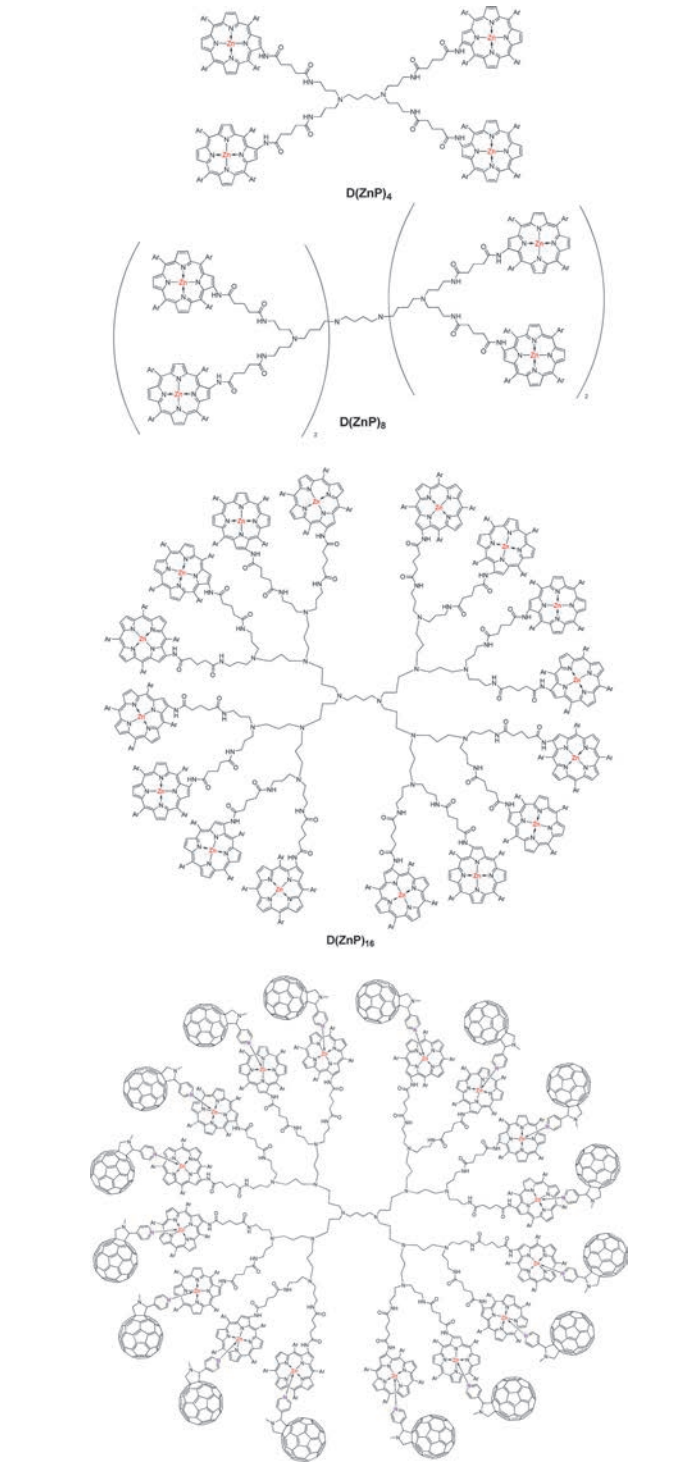

Chart 2 Chemical structures of porphyrin dendrimers and a coordination complex with 16 fullerene units.[60]

In a system designed by Hupp and coworkers, a ladder coordination motif was achieved, which exhibited electron transfer abilities. A zinc porphyrin trimer connected by butadiynylene units *via* the *meso*-positions of porphyrins was prepared, which acted as the rail of the ladder. Two of these rail molecules were coordinated to three dipyridyltetrazine or

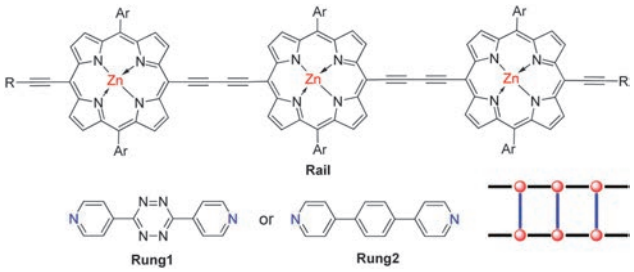

Chart 3 Chemical structures of zinc porphyrin trimer, dipyridinylbenzene, and dipyridinyltetrazine, and a schematic illustration of their ladder-shaped complexes.[61]

dipyridylbenzene ligands (as the rung), affording a self-assembled ladder-shaped complex in toluene solution.[61] The binding stoichiometry of these complexing partners was confirmed to be 2 : 3. Photo-induced electron transfer was found to occur from the excited porphyrin to a tetrazine at one end of the ladder. With the remaining hole delocalized over the three porphyrins, a charge separated state lifetime of 0.19 ns was determined (Chart 3).

2.2 Assemblies driven by aromatic stacking and solvophobic interactions among π-systems

While using metal–ligand coordination interactions is a more faithful mimic to the natural photosynthetic system, π–π stacking is nonetheless a more commonly occurring non-covalent interaction in photoactive molecular assemblies. Importantly, the face-to-face aggregation motif of aromatic structures resulting from π–π interactions is compatible with intermolecular charge transport functions. Namely, with proper chemical and assembling structures, not only charge separation but also photocurrent can be achieved in π–π stacked molecular assemblies.

Hexabenzocoronene (HBC) is a widely studied aromatic group exhibiting a strong tendency to aggregate face-to-face, since its large polycyclic π-framework imparts a significant π–π stacking force. Its various derivatives have been observed to self-aggregate into columnar structures, which under proper conditions exhibit prominent hole transport semiconductive abilities.[62] Müllen, Friend and coworkers first reported the photovoltaic effect of a columnar liquid crystalline hexaphenyl HBC (**HBC–PhC12**), which upon blending with perylene diimide, generated a photocurrent under the illumination of 490 nm light, evidencing that charge separation and transport were realized in the phase-segregated film.[63]

In 2004, Aida and co-workers reported the self-assembly of a diphenyl substituted amphiphilic HBC (**HBC-1**) into hollow nanotubes in solution.[64] This molecule features a less symmetric shape, with two long alkyl side chains appended to one side of HBC and tri(ethyleneglycol)-substituted diphenyls on the opposite side. This molecule was found to form double-layered nanotubes, as the thickness of the tube wall was approximately twice the length of a HBC monomer. In view of such a unique supramolecular architecture, the authors then designed a series of derivatives with related chemical structures

and carried out a systemic investigation to reveal the key structural parameters that govern the self-assembly behaviors.[65]

The results showed that the steric hindrance caused by the two *p*-phenylene substituents on HBC and the unsymmetric molecular shape both held great responsibility for the emerged slightly skewed stacking motif in the aggregates. Consequently, a twisted tubular structure rather than a columnar arrangement occurred. The two long alkyl side chains on HBC were also indispensable, which interdigitated intermolecularly inside the wall to support the double-layered assembling motif, as well as contributing to the overall stability of the tubes. The hydrophilic oligo(ethylene-glycol) side chains were non-critical for nanotube formation, since the tubular structure still persisted upon removal of these hydrophilic chains.[65] Nonetheless, these ethylene glycol chains afforded adequate solubility and thus helped the tubular assemblies remain individually dispersed in solution.

The major driving force for the intermolecular stacking of these HBC derivatives was proposed to be the π–π interactions among the HBC moieties. The solvents, including THF and methanol, created a solvophobic environment for both the aromatic framework and alkyl chains. Nonetheless, for certain studied HBC analogues, self-assembled nanotubes were even detected in CH_2Cl_2.[65] This observation verified the very strong stacking ability of HBC, since CH_2Cl_2 is typically considered a good solvent for aromatic structures.

Two-dimensional X-ray diffraction (2D-WAXD) of the aligned nanotubes of **HBC-2** revealed that the stacking direction of HBC was along the tube long axis, which is viable for establishing charge transport (Fig. 1). Electron acceptors with a low-lying LUMO were then attached to the end of a tri(ethylene-glycol) chain on the HBC monomers, in order to promote photo-induced electron transfer and generate charge carriers (*i.e.*, holes in HBC and electrons in the acceptor moieties). For example, **HBC-3**, a trinitrofluorenone (TNF) moiety was utilized as the acceptor.[66] The self-assembly of **HBC-3** was induced by diffusing methanol vapor into a THF solution. Nanotubes with a highly uniform diameter (16 nm) and wall thickness (3 nm) were observed in a yellow suspension. The self-assembly conditions were reported to require subtle tuning and control in order to obtain the ordered tubular aggregates of **HBC-3**. An inappropriately high initial concentration of **HBC-3** in THF solution would result in precipitates comprising microfibrils

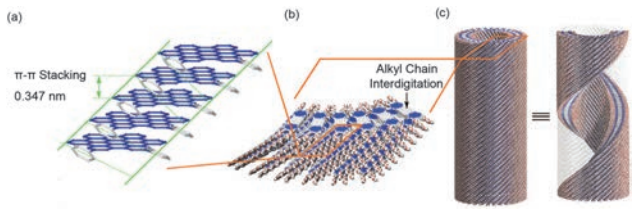

Fig. 1 Schematic representation of the hierarchical self-assembly of **HBC-2**. (a) π-Stacked columnar array, (b) bilayered wall, and (c) nanotube. (Adapted with permission from ref. 65. Copyright © 2008 American Chemical Society.)

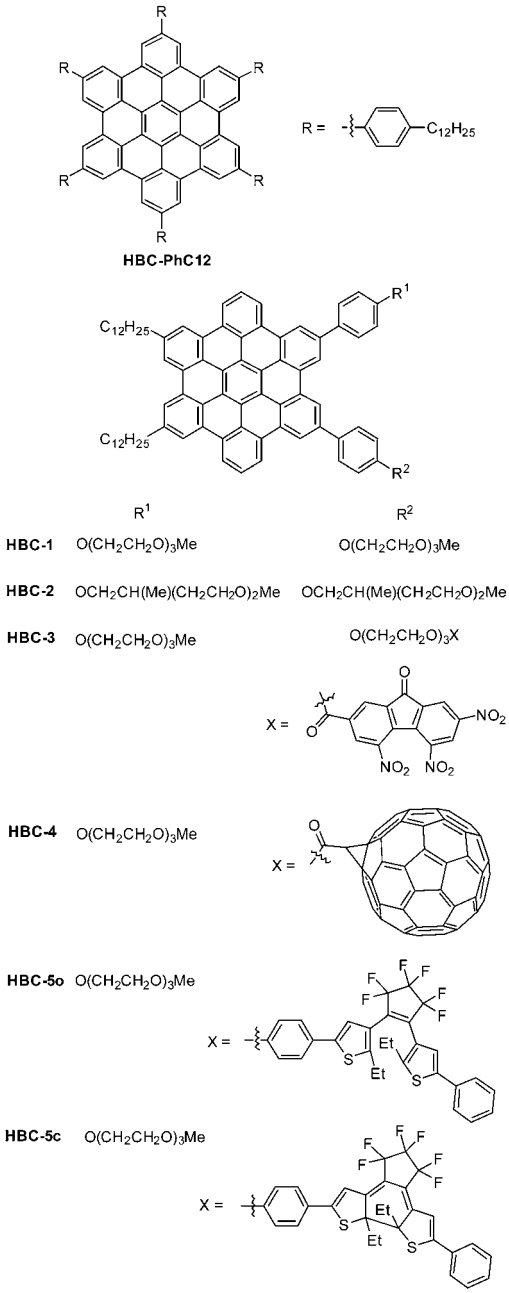

Chart 4 Chemical structures of HBC derivatives.[64–68]

without the hollow interior. Since the structural characteristics of **HBC-3** were highly similar to those of **HBC-2**, the formed nanotubes were proposed to possess common supramolecular features, except that a layer of TNF was coating the exterior of the double-layered nanotubes of **HBC-3**. Therefore, redox pairs were spatially segregated and presumably formed separated aggregation domains (Chart 4).

The nanotubes of **HBC-3** on a silicon substrate exhibited a photocurrent upon irradiation, with a large current on/off ratio of over 10^4. The detection of photocurrent further proved the presence of bicontinuous carrier transport pathways in the nanotubes. The aggregation morphology was also important

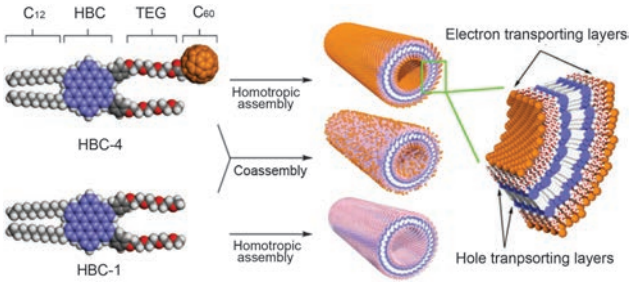

Fig. 2 Schematic representation of homotropic and co-assembled nanotubes of **HBC-1** and **HBC-4**. (Adapted with permission from ref. 68. Copyright (2009) National Academy of Sciences, USA.)

for the photoconductivity, as no photocurrent was detected for the microfibrils formed by the same molecule at higher concentrations. As a control, nanotubes of **HBC-1** showed minimal photocurrent under the same conditions.

Compared with TNF, fullerene derivatives are more commonly employed as electron acceptors. Driven by aromatic interactions, C_{60} has a perceptible tendency to form aggregates. Clusters of C_{60} thus have prominent electron transporting abilities. Further optimizations of Aida's HBC system involved covalently connecting a studied HBC molecule with fullerene to create a D–A dyad. Accordingly, the designed **HBC-4** was also found to form nanotubes, with a diameter of 22 nm and wall thickness of 4.5 nm (Fig. 2).[68] The substantial fluorescence quenching of HBC in the presence of the C_{60} group suggested effective charge separation in the nanotubes of such a dyad. The C_{60} moieties were deemed to form a continuous acceptor layer covering the nanotube exterior. Impressively, nanotubes of **HBC-4** exhibited ambipolar semiconductive properties in the field-effect transistor, evidencing the competent hole and electron transporting abilities of HBC and C_{60}, respectively. Moreover, **HBC-4** could co-assemble with **HBC-1** at varied ratios to form nanotubes under respectively optimized conditions. Photovoltaic effects were observed with such co-assemblies of **HBC-1** and **HBC-4**. The best performance was achieved at a given ratio, presumably when a balanced electron and hole mobility was offered.

In addition to DNF and C_{60}, another examined acceptor group was dithienylethene (DTE). A unique property of this moiety is that it undergoes a reversible ring-closure and ring-opening isomerization reaction under the illumination of UV and visible light, respectively. Molecules **HBC-5o** and **HBC-5c** maintained the ability to self-assemble into similar nanotubular structures as **HBC1-4**,[67] and the reversible cyclization/ring-opening reaction was also proven to proceed properly in the aggregated state. Interestingly, the photoconductivity of the nanotubes increased by a factor of 5 after the DTE pendants underwent the ring-closure reaction. Such a phenomenon was proposed to arise from the varied electron affinity of DTE in different isomer forms. Different numbers of charge carriers were produced in **HBC-5o** and **HBC-5c**, resulting from the different HBC-to-DTE electron transfer efficiencies. Thereby, a novel photoconductivity modulation mechanism by a photochromic switch was realized, which implied a prototype of a multimode photo-responsive nanomaterial.

It can be perceived from the above system that nanotubes of very similar supramolecular structures were repeatedly and reliably reproduced by different HBC derivatives appended with varied functional groups. Such a high consistency in the aggregated structure indicated the inherently high structural stability of HBC aggregates, benefitting from both the large aromatic stacking surface of HBC, as well as the non-negligible reinforcing lipophilic interactions among the interdigitated long alkyl chains. Another reason for the consistent nanotube formation is that the acceptor groups were not strongly interfering with the aggregation of HBCs.

However, for most dyad molecules, bicontinuous donor–acceptor phases and separated charge transport pathways are not as readily attained. This is because the donor and acceptor groups in the dyads are usually both aromatic structures and prone to undergo aromatic stacking in an alternating fashion upon aggregation, due to charge transfer characteristics. Such a mixed packing motif of donor and acceptor is however not favorable for charge separation or transport.

Designing amphiphilic dyads has proven to be an effective tactic to suppress such charge-transfer complexes. For example, if donor and acceptor moieties in the dyad molecules are decorated with side chains of distinct chemical features and different solvent affinities, *e.g.*, hydrophilic *vs.* hydrophobic, the respective self-aggregation of donor and acceptor groups likely becomes the thermodynamically favored state in suitable solvents, giving rise to phase segregated assembly structures. Further, although the aggregations of donors and acceptors are both dictated by aromatic stacking, they can be tuned by van der Waals interactions among the side chains.

Amphiphilic dyad design is well demonstrated by **Th–C60-1** and **Th–C60-2**.[69] In these molecules, oligothiophene and C_{60} were connected *via* an ester linkage, serving as the electron donor and acceptor, respectively. The only difference between the two dyads lies in the side chains. In **Th–C60-1**, a phenyl group bearing multiple aliphatic dodecyloxy side chains was attached to the end of an oligothiophene chain, while hydrophilic triethylene glycol chains were tethered to the side of C_{60}, conferring an amphiphilic character to this molecule. But for **Th–C60-2** both oligothiophene and C_{60} were decorated with hydrophobic dodecyloxy groups. In the smectic liquid crystalline phase, amphiphilic **Th–C60-1** was found to produce highly ordered bicontinuous donor stacks of oligothiophene and acceptor stacks of C_{60}, forming a bilayer architecture, whereas **Th–C60-2** generated a much less ordered monolayer structure, with significant mixing of the aliphatic side chains from the opposite side of the molecule. These differences in the molecular ordering were characterized by small-angle X-ray scattering (SAXS). The different molecular packing brought about quite distinct photoactivities. The photocurrent generated by **Th–C60-2** was only 1/10 of the magnitude detected for **Th–C60-1** under the same conditions. Experimental evidence was also obtained showing that charge carriers generated by **Th–C60-2** had a shorter lifetime than those in **Th–C60-1**, suggesting the

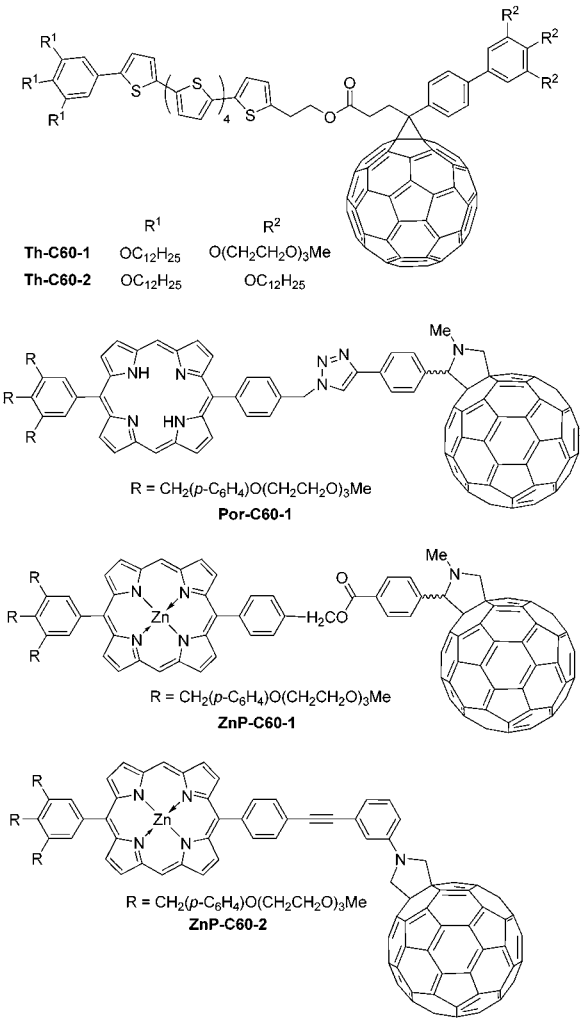

Chart 5 Chemical structures of donor–acceptor dyads.[69–72]

presence of a larger number of trapping sites in the former (Chart 5).

A more subtle dependence on the chemical structure is manifested by the aggregation motifs when the amphiphilic character of the dyads becomes less pronounced. This concept is well demonstrated by the following system. In the dyad **Por–C60-1**, diphenylporphyrin was employed as the donor group to complement the electron acceptor fullerene. While the donor segment was still tethered with three hydrophilic triethylene glycol tails, the side chains on the fullerene side were removed. Apparently, in this case the major driving force for molecule aggregation was still π–π interactions among the large aromatic backbone comprising the bridged porphyrin and fullerene.[72] In this dyad molecule, the acceptor (fullerene) moiety was connected to the donor (diphenylporphyrin) *via* a covalent spacer containing a stereogenic center. This study demonstrated that even the identity of the stereo center sensitively influenced the molecule aggregate structure, which in turn dictated the viability of photoactivity.

The self-assembly of relevant molecules into ordered supramolecular structures was achieved by diffusing methanol into CH_2Cl_2 solutions of **Por–C60-1**. The former was a poor solvent, promoting aromatic stacking and solvophobic interactions among the hydrophobic backbone. While racemic **Por–C60-1** formed nanospheres of 300 nm in diameter, which were not photoconductive, enantio-pure (+)- **Por–C60-1** self-assembled into bundles of nanofibers with lengths of up to 10 μm and widths of several hundred nanometers. When the nanofibers of (+)- **Por–C60-1** were exposed to Xe light (300–650 nm), a photocurrent was detected, which was immediately shut off upon removal of light irradiation. The fact that the self-assembled nanofibers of (+)- **Por–C60-1** were photoconductive is actually quite impressive. The generation of a photocurrent necessarily relied on the presence of segregated donor and acceptor groups in the nanofibers, but achieving separated hole and electron transport pathways in such a molecule was imaginably difficult, since the attractive forces between the Zn-porphyrin and fullerene[70] moieties were notably strong due to the charge-transfer character.

Further studies revealed that a subtle chemical linker change in the dyad backbone also strongly influenced the aggregate structure. The ester-linked dyad **ZnP–C60-1** and acetylene-linked dyad **ZnP–C60-2** were subsequently examined regarding their intermolecular aggregation behaviors and photoactivities.[71] Suitable conditions for the self-assembling dyad **ZnP–C60-1** were first identified, which entailed adding methanol to a toluene solution. Subsequently, the molecule **ZnP–C60-1** self-aggregated into nanotubes with a uniform diameter of 32 nm and wall thickness of 5.5 nm. By comparing the wall thickness with the molecular size of the dyad monomer, the aggregates were proposed to assume a bilayer structure. Under such solvent conditions, clustered C_{60} units were most likely buried inside the tube wall, surrounded on both sides by stacked Zn-porphyrins, while the polar side chains were coated on both the inner and outer surfaces of the tubes (Fig. 3). In contrast, based on the SEM and TEM images, the nanotubes formed by the acetylene-linked dyad **ZnP–C60-2** displayed much smaller tube diameters (7–8 nm), along with an estimated wall thickness of only 1.7–1.8 nm. Since the wall thickness was only slightly shorter than the end-to-end distance of the molecule, a model of a mono-layered aggregate was proposed, in which **ZnP–C60-2** was oriented in a tilted fashion (Fig. 3). Further, in the nanotubes of **ZnP–C60-2**, the Zn-porphyrin and C_{60} units were not segregated but instead stacked on top of one another, forming an alternating D–A array. Such a conclusion was consistent with the photoconductive performance of the aggregates formed by the two molecules. The nanotubes of **ZnP–C60-1**, with a segregated D–A heterojunction displayed a much higher photoconductivity than **ZnP–C60-2**, having an alternating D–A arrangement. Specifically, the **ZnP–C60-1** nanotubes displayed photovoltaic responses with an open-circuit voltage of 0.66 V and short-circuit current of 16 pA, while under identical conditions the corresponding values from the aggregated **ZnP–C60-2** were only 0.16 V and 0.9 pA, respectively. Again, such distinct molecular assembling motifs yielded by **ZnP–C60-1** and **2** clearly illustrate

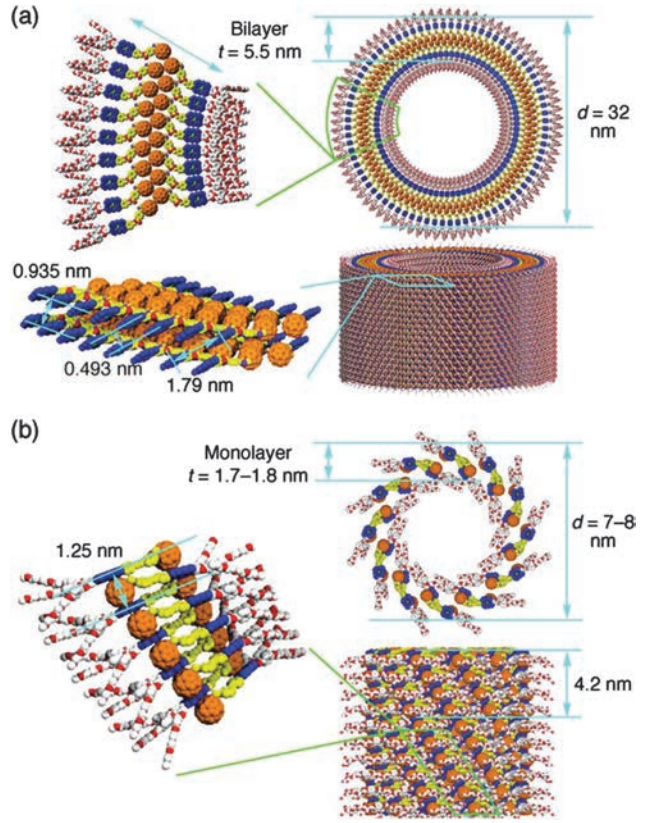

Fig. 3 Schematic representations of tubular assemblies of **ZnP–C60-1** (a) and **ZnP–C60-2** (b). (Reprinted with permission from ref. 71. Copyright (2012) American Chemical Society.)

the subtlety and power of chemical structures in dictating the supramolecular architectures of molecular assemblies.

In addition to fullerene derivatives, dicarboximides such as perylenediimide (PDI) and naphthalenediimide (NDI) are also commonly studied as electron acceptors. In these systems, side-chain modulated aggregation behaviors have similarly manifested, for example by oligothiophene–PDI dyads of amphiphilic **Th–PDI-1** and lipophilic **Th–PDI-2**.[73] In dilute solutions of CH_2Cl_2 where the dyads were molecularly dispersed, the fluorescence of both molecules was completely quenched, suggesting the occurrence of photo-induced electron-transfer between the oligothiophene donor and PDI acceptor moieties. However, different properties were exhibited in the aggregated state. Amphiphilic **Th–PDI-1** generated nanofibers with segregated donor–acceptor moieties, while **Th–PDI-2** having lipophilic side chains on both ends of the molecule formed ill-defined microscopic fibers with disordered donor–acceptor arrangements. The disparate phase separation features were evidenced by the distinct photoactivities of the two molecules. Under identical conditions, photocurrent generated from the assembled **Th–PDI-1** was three orders of magnitude larger than that from aggregated **Th–PDI-2** (Chart 6).

Completely planar, electron-deficient aromatic frameworks, such as PDI and NDI, typically exhibit very strong π–π stacking interaction strengths, evidenced by their poor solubility in most

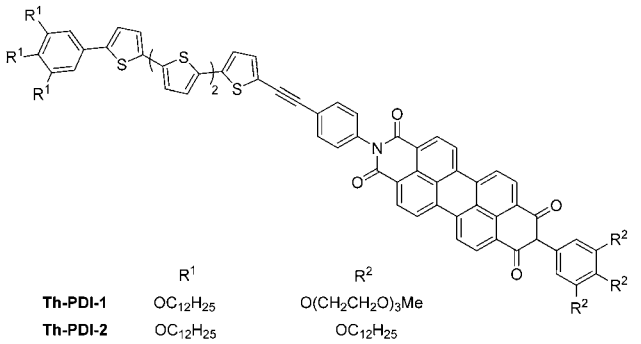

	R^1	R^2
Th-PDI-1	$OC_{12}H_{25}$	$O(CH_2CH_2O)_3Me$
Th-PDI-2	$OC_{12}H_{25}$	$OC_{12}H_{25}$

Chart 6 Chemical structures of oligothiophene–PDI dyads.[73]

organic solvents.[74] Such strong stacking forces are now well recognized and frequently used to create supramolecular assemblies.[49,50,75,76] Parquette and co-workers studied the aggregation behaviors of a series of NDI derivatives with hydrophilic side chains.[77–81] Symmetric **NDI1** was tethered with two amino acids *via* a segment of the aliphatic side chain on both imide nitrogen atoms.[80] Experimental evidence was obtained showing that nano-rings were formed by this amphiphilic molecule in water. In these nano-rings, NDIs were packed face to face driven by π–π stacking interactions, while the hydrophilic amino acids were positioned on both the interior and exterior of the ring, being exposed to the polar solvent molecules (Fig. 4). These nano-rings then stacked into nanotubes, with relatively uniform diameters and lengths of over 1 μm. A more interesting self-assembly structure was shown by **NDI2** bearing only one amino acid side chain. Although this molecule also formed nano-rings in aqueous solution, a

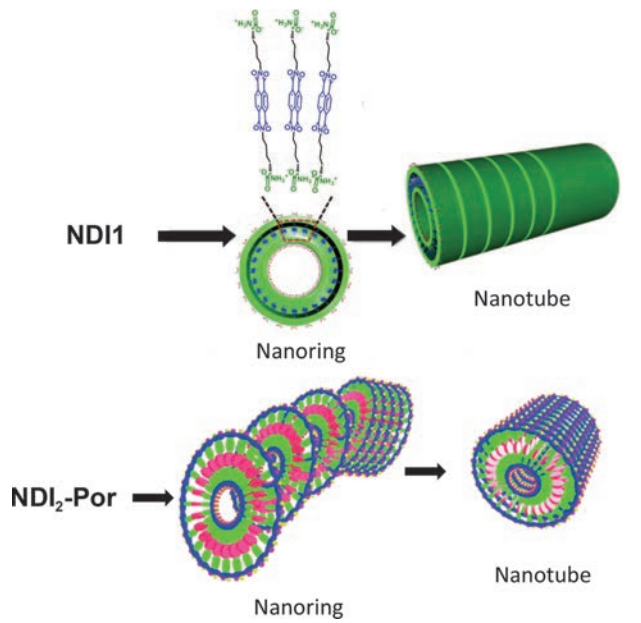

Fig. 4 Chemical structures and schematic illustration of assembly process of **NDI1** and **NDI_2–Por**. (Adapted from ref. 80 Copyright © 2010 WILEY-VCH Verlag GmbH & Co. KgaA, Weinheim & ref. 81. Copyright © 2011, American Chemical Society.)

bilayered model was proposed, in which the hydrophobic alkyl chains were oriented toward the inside and the polar amino acid heads were arranged at both the outer and inner rims of the ring.[77] Moreover, these bilayered nano-rings were observed to further self-assemble into long, twisted ribbons and helical tapes, which were still intermediate states eventually leading to nanotubes. This process clearly unraveled how a hierarchical tubular supramolecular architecture evolves from basic molecular building blocks.

In order to confer photoactivity to such uniquely self-assembled supramolecular structures, a porphyrin–NDI dyad (**NDI_2–Por**) was then designed and investigated.[81] Two NDI units, each tethered with an amino acid at the side chain terminal, were ligated to the opposite side of a tetraphenylporphyrin. As expected, in an aqueous solution containing 10% methanol, **NDI_2–Por** formed nano-rings with a monolayer structure, manifesting eminent *J*-type exciton coupling characteristics in the absorption spectrum. These nano-rings could further assemble into nano-tubular architectures under neutral conditions. Photo-induced electron transfer from porphyrin to NDI moiety was detected within the nanotubes by transient absorption spectroscopy. However, under either basic or acidic conditions, where the amino acid was negatively or positively charged, the nanotubes were disrupted, and nonspecific aggregates with ill-defined structures were observed. This phenomenon apparently resulted from repulsions between charged amino acids, which disrupted the π–π stacking interactions among NDI units and hence altered the aggregate structures (Chart 7).

2.3 Self-assembled molecular aggregates with multiple noncovalent driving forces

As seen from previous examples, noncovalent interactions, particularly π–π stacking, can be conveniently incorporated into design schemes in creating supramolecular architectures and realize desired photo-functions. As illustrated by the following systems, since these noncovalent bonds are usually orthogonal and non-interfering with one another, one can simultaneously deploy more than one type of them into a single supramolecular system. With greater flexibility in the employable noncovalent interactions, the structures of incorporated modular building blocks as well as the assembling motifs can be further diversified, which is evidently favorable for improving the functional performance of the system.

2.3.1 Hydrogen bond-assisted π–π stacking assemblies. In addition to metal–ligand coordination and π–π stacking interactions, hydrogen bonding (H-bonding) is another important noncovalent force frequently used in building supramolecular assemblies. The hydrogen bond (H-bond) is a relatively robust type of noncovalent interaction.[51] Another distinct advantage of H-bonding is that there is a wide range of different H-bonding structures available for use (Chart 8).[52]

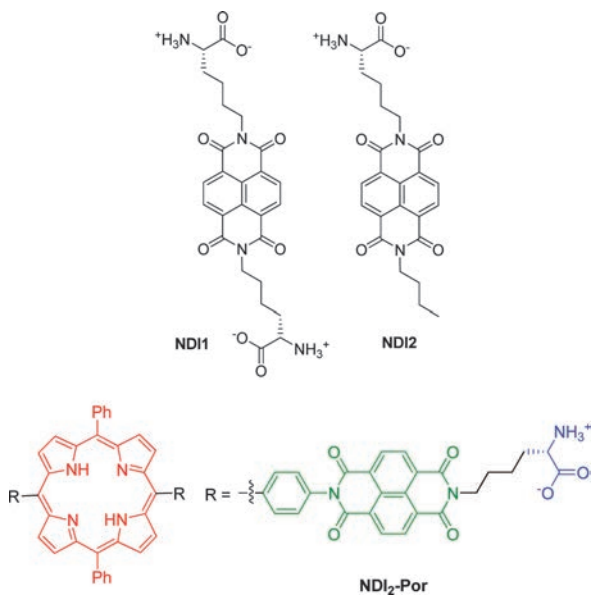

Chart 7 Chemical structures of amphiphilic NDI derivatives.[77–81]

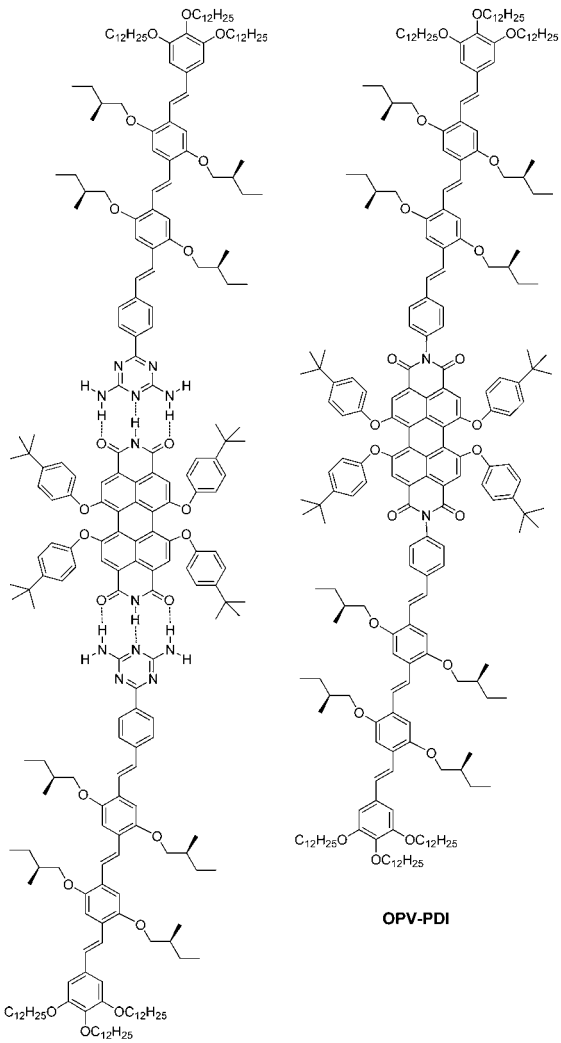

Chart 8 Chemical structures of **OPV:PDI** and **OPV–PDI**.[82,83]

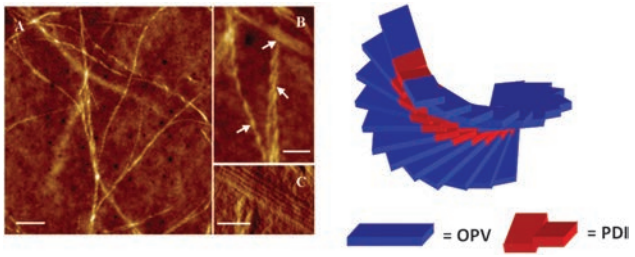

Fig. 5 Left: tapping mode AFM topographic images of **OPV:PDI** triad from spin-coating MCH solution on a glass//PEDOT:PSS slide (scale bars: 500 nm in A, 100 nm in B and 50 nm in C). Right: helical stacking model for **OPV:PDI** triad composed of **OPV** and *M*-enantiomer of **PDI**. (Adapted with permission from ref. 83. Copyright (2004) American Chemical Society.)

Meijer, Würthner and coworkers collaborated on studying the self-assembly of a supramolecular triad (**OPV:PDI**) containing oligo(phenylenevinylene) and PDI as donor and acceptor partners. The unique character of this system is that the triad monomer **OPV:PDI** is a supramolecular object, featuring an ADA–DAD triple H-bond linkage between the donor and acceptor groups.[82,83] In the acceptor portion, **PDI** inherently possessed two ADA-type H-bonding moieties (*i.e.*, imide group), while in the donor part, a diamino-triazene group offering a complementary DAD H-bonding motif was attached to the end of the oligo(phenylenevinylene) chain. Thus, a supramolecular donor–acceptor–donor triad was conveniently obtained upon mixing **OPV** with **PDI** in a suitable solvent, driven by H-bond formation. The π–π stacking interactions among these supramolecular triads then promoted hierarchical aggregation in methylcyclohexane (MCH) solution (Fig. 5). This solvent selectively solvated the alkyl side chains on both **PDI** and **OPV**, but was incompatible with the aromatic backbone of the H-bonded triad, resulting in strengthened π–π stacking. Long, helically twisted nanofibrils were afforded by this co-assembled supramolecular system. Transient absorption spectroscopy proved that photo-induced electron transfer occurred between the electron donor **OPV** and acceptor **PDI** in the π–π stacked aggregates.

For a comparison study, a covalently linked triad **OPV–PDI**, consisting of very similar subunits to **OPV:PDI**, was synthesized. A major difference in the molecular conformation arose between **OPV:PDI** and **OPV–PDI**. Due to the imide nitrogen linkage, the **OPV** segment in **OPV–PDI** had to assume a dihedral angle with respect to the **PDI** moiety, while in the H-bonded **OPV:PDI** a coplanar conformation was adopted by the two subunits. Subsequent studies revealed important structural differences between the aggregates formed by these covalent and noncovalent analogues. As shown by the absorption spectra, a stronger exciton coupling effect was observed with **OPV:PDI** than **OPV–PDI**, suggesting a more intimate molecular stacking occurred with the H-bonded aggregate. This is a consistent result with the more planar conformation of **OPV:PDI**, which is favorable for tighter π–π stacking. Additionally, a faster back electron transfer rate was detected from the

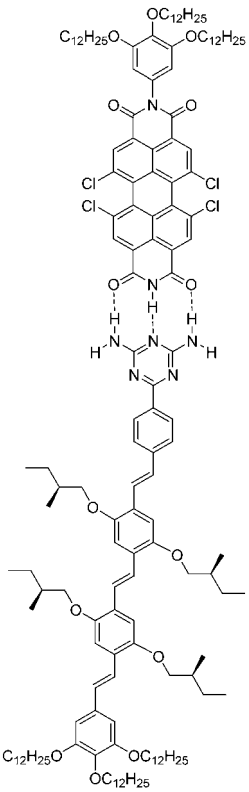

OPV:PDI2

Chart 9 Chemical structure of **OPV:PDI2**.[84]

charge separated state of the aggregated **OPV:PDI** than that of the aggregated **OPV–PDI**. This should also be related to the coplanar conformation and more compact stacking of **OPV:PDI** (Chart 9).

A H-bonded dyad analogue **OPV:PDI2** was subsequently designed.[84] In addition to switching from a triad to a dyad, a more important chemical modification was that the four electron-donating tetraphenoxy substituents on PDI in **OPV:PDI** were replaced with four more electro-negative chlorine atoms. This structural alteration had important consequences. First, it boosted the electron-accepting ability of the PDI unit by lowering its LUMO, which was favorable for electron transfer. Moreover, the electron transporting ability of the acceptor domain in the aggregate was greatly improved as well, since the less bulky chlorine atoms allowed for more compact π–π stacking and more effective intermolecular orbital coupling among the PDI units, favorable for charge migration. AFM characterization for solution-cast thin films of **OPV:PDI2** revealed a morphology with nano-scale phase separation features, and the field effect transistor further demonstrated the ambipolar charge transporting ability of the aggregated **OPV:PDI2** in the thin-film state.[84]

2.3.2 Zinc chlorin rods formed *via* π–π stacking, hydrogen bonding, and metal oxygen coordination. A particularly elaborate photoactive aggregate system (**ZnCh1–6**) was developed by Würthner and co-workers, utilizing a combination of

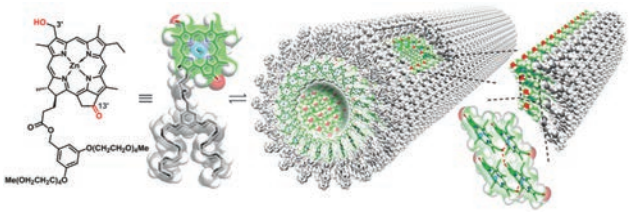

Fig. 6 Schematic model of self-assembled nanotubes formed by **ZnCh3**. (Adapted with permission from ref. 88. Copyright © 2012 WILEY-VCH Verlag GmbH & Co. KgaA, Weinheim.)

π–π stacking, H-bonding, and metal–oxygen coordination interactions.[85] Based on the results from prior studies,[75] semisynthetic zinc chlorin derivatives **ZnCh1–3** formed macrocyclic self-aggregates, in which the oxygen atom of the 3′-hydroxyl was coordinated to zinc from an adjacently stacked chlorin. The thus formed molecular arrays featured a slipped stacking arrangement of chlorins, favoring π–π stacking interactions. In the meantime, the 3′-hydroxyl group was H-bonded to a 13′-carbonyl of another molecule from a different stack. *J*-Type exciton coupling among the aggregated chlorins was evidenced by the large bathochromic shift observed in the absorption spectra.[86,87] Building upon such aggregated structures, molecules **ZnCh1–3** formed discrete nanorods in water. Particularly, the amphiphilic **ZnCh3** exhibited well-defined aggregate structures with a diameter of 6 nm and lengths of several micrometers (Fig. 6). Most notably, evident photoconductivity was detected for the nanorods of **ZnCh1–3**, based on measurements conducted by pulse-radiolysis time-resolved microwave conductivity (TRMC) and conductive AFM measurements (Chart 10).[75,88]

In the further developed dyads **ZnCh4–5** and triad **ZnCh6**, chlorin derivatives were ligated to NDI with alkoxyl or amino substituents *via* relatively flexible linkers.[89] The main purpose of decorating these NDI units with different substitution patterns was to bestow them with the ability to serve as light harvesting antenna, complementing the absorption of chlorin by broadly covering the 500–600 nm region. The self-assembly of **ZnCh4–6** was carried out in nonpolar aprotic solvents. *J*-Aggregates were formed by chlorin moieties in all three molecules, while the tethered NDI units remained dispersed in aqueous solution (Fig. 7). Highly efficient Förster resonance energy transfer (FRET) took place from the visible-absorbing NDI groups to the ''green trap'' of chlorin, *via* a single-step photon transfer in **ZnCh4–5**, and a sequential two-step FRET in **ZnCh6**.

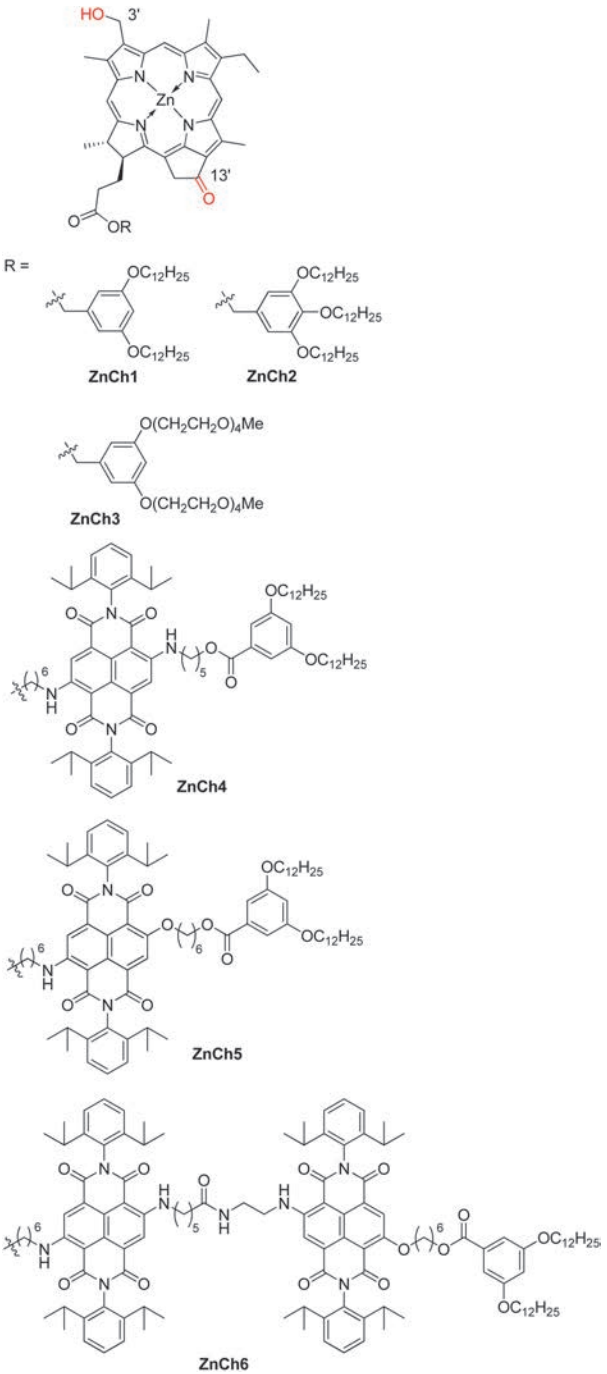

Chart 10 Chemical structures of zinc chlorins.[86,87,89]

2.4 Supramolecular assembly-facilitated covalent scaffold constructions

In spite of the appealing properties of supramolecular architectures, covalent bonds after all afford the ultimate chemical stability. Thus, properly combining covalent ligation with supramolecular forces offers the most versatile and reliable approach to constructing sophisticated hierarchical functional systems, in which covalent bonds provide robust scaffolds with optimal chemical stability while noncovalent interactions offer the structural flexibility, allowing for strain release. Furthermore, even the abilities of self-healing or self-correction may be imagined with supramolecular interaction-facilitated covalent syntheses, by virtue of the reversibility and fidelity offered by noncovalent recognition processes. Such examples are perfectly demonstrated by the natural macromolecule systems. Namely, all replication, transcription, and translation processes in the central dogma rely on the ''templating'' effects, essentially noncovalent interaction-facilitated covalent syntheses, to

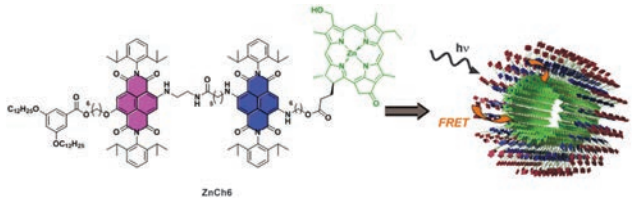

Fig. 7 Illustration of the rod-like *J*-aggregate model of **ZnCh6** with arrows indicating the light absorption and FRET. (Adapted with permission from ref. 85. Copyright (2013) American Chemical Society.)

realize sequence control. A similar strategy of harnessing noncovalent interactions to facilitate the ligation of covalent bonds has been applied to synthetic systems (Chart 11).[90,91]

When a similar approach is employed in photoactive macromolecule design, it opens up numerous new opportunities for developing relevant functional systems. An outstanding example of combining noncovalent forces with covalent bonds to devise photoactive arrays was realized by Matile and coworkers. The evolution of the design started with noncovalent assemblies. They first recruited a rigid oligophenylene as the backbone. To each repeating unit on this backbone was tethered a NDI unit *via* an amide linkage (**Ph-NDI1**–**3**).[93] The initiator **Ph-NDI1** was first coated onto a gold substrate by a Au–S bond. This monolayer was then exposed to cationic **Ph-NDI2** (a propagator). Driven by the π–π stacking interactions among the NDI units and electrostatic attraction between the terminal

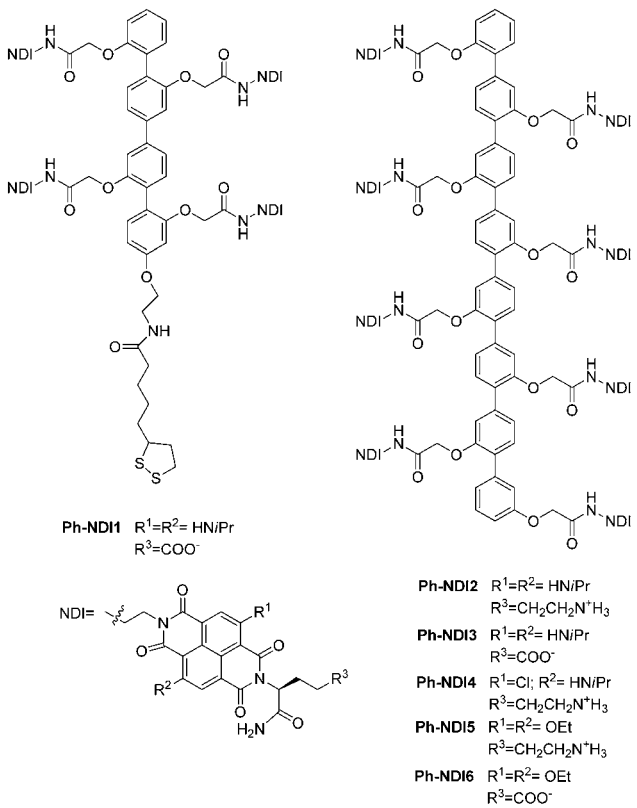

Chart 11 NDI "zippers" with an oligophenylene backbone.[92–94]

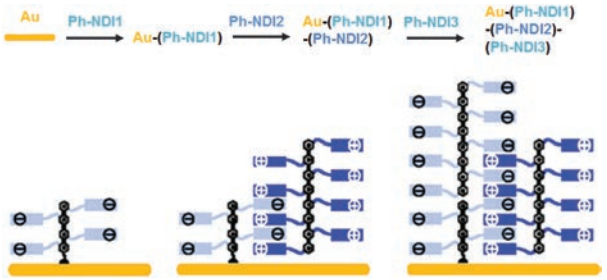

Fig. 8 Illustration of zipper assembly on a Au electrode. (Adapted with permission from ref. 93. Copyright (2007) American Chemical Society.)

anionic carboxylate and cationic ammonium groups on **Ph-NDI1** and **Ph-NDI2**, as well as the H-bonds formed between the amide functionalities, a second layer of molecules was deposited onto the substrate. As the length of **Ph-NDI2** mismatched that of **Ph-NDI1**, "sticky-ends" were exposed in the upper part of **Ph-NDI2**. Then, the other propagator **Ph-NDI3** with negatively charged terminal groups was applied and assembled with the exposed segment of **Ph-NDI2**, driven by the same types of noncovalent interactions joining **Ph-NDI1** and **2**, *i.e.*, electrostatic, H-bonding and π–π stacking forces. Such propagation cycles were repeated several times to form a multi-layered structure on a Au electrode (Fig. 8). Each deposition cycle was monitored by examining the absorption of NDI at *ca.* 630 nm. With the Au electrode as the electron acceptor, photoconductivity measurements were performed on the zipper assembly, which unambiguously exhibited progressively increased photocurrents upon propagation. The magnitude of detected photocurrents was much larger than that from assemblies prepared *via* the layer-by-layer technique.

To further tune the photoconductivity of such a zipper assembly, another oligophenylene supported NDI propagator **Ph-NDI4** with a stronger electron affinity (lowered LUMO) was designed,[94] and a cascade zipper assembly of Au–(**Ph-NDI1**)–(**Ph-NDI4**)–(**Ph-NDI3**)–(**Ph-NDI2**) was attained. The current–voltage curves of this new zipper assembly showed a perceptibly improved V_{oc} and FF values. By further introducing **Ph-NDI5–6** with even lower LUMO levels, an energy-favored electron transport array was attained by lining up different molecules in the order of increasing electron affinity. Therefore, more efficient photo-induced electron transfer and a long-lived charge separated state were achieved.[92] The combined absorption spectra of all NDIs also covered the entire visible light range, making them a potentially useful chromophore array for artificial photosynthesis (Chart 12).

Oligophenylene was nonetheless not the ideal scaffold for such zipper assemblies, because of the mismatched repeating-unit length (*ca.* 0.5 nm) and the π–π stacking distance (0.35 nm). Oligo-*para*-phenyleneethynylene (OPE), with a repeating unit length of *ca.* 0.7 nm, was considered a superior choice.[95] Moreover, OPE was also a better electron donor with a planarizable backbone. The OPE-supported NDI zipper molecule **OPE-NDI1-3** was then synthesized and applied to form the zipped assemblies in a configuration of Au–(**OPE-NDI1**)–((**OPE-**

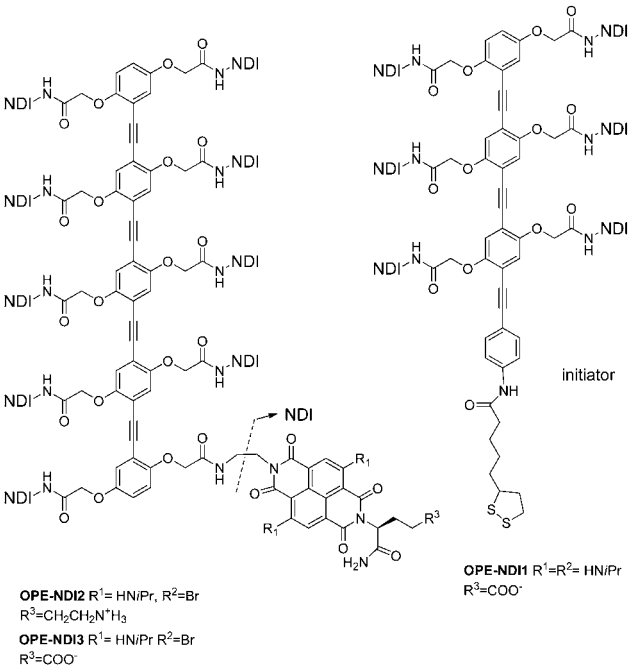

Chart 12 NDI "zippers" with OPE backbone.[95]

NDI2)–(**OPE-NDI3**))$_n$. With these assemblies, the photocurrent density increased almost linearly with the number of deposited layers, until reaching saturation at about 20 layers. Under the same conditions, oligophenylene-supported zippers gave only about a 60% increase in the photocurrent per layer.

In the above systems, the assembled molecules were "zipped" together by supramolecular forces. In order to anchor the entire assembly covalently to the substrate and build a more robust conductor system, the authors further developed a new protocol named self-organized surface-initiated polymerization (SOSIP).[96] Reduction of the disulfide groups in the initiator **NDI1** with dithiothreitol (DTT) liberates reactive thiolates on the ITO surface. Then, a ring-opening disulfide exchange polymerization is initiated (Scheme 1). Recognition of the

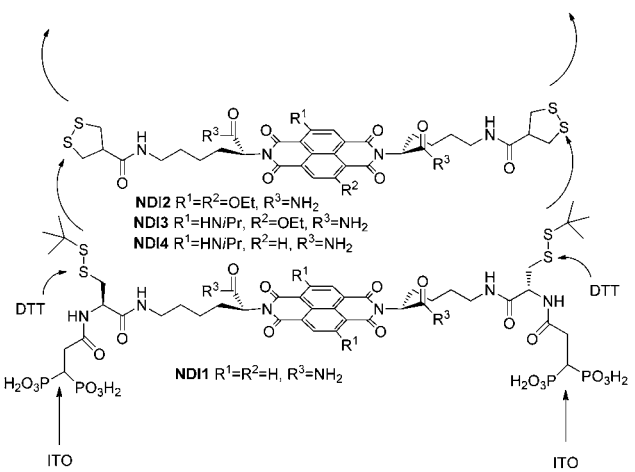

Scheme 1 Surface-initiated polymerization of NDIs.[96]

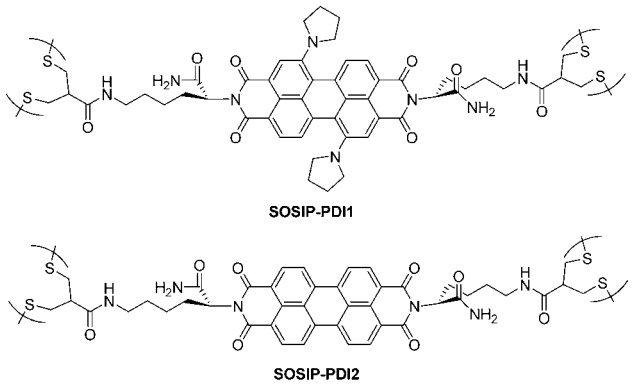

Chart 13 SOSIP PDI stacks.[96,97]

propagators **NDI2–4** by the prior co-monomer was again realized through supramolecular interactions, including H-bonding between amide groups and π–π stacking between NDI units. The photocurrent generated by ITO–**NDI1**–(**NDI2**)$_n$ was 5 times larger than that of a disordered system. A more complex assembly of ITO–**NDI1**–(**NDI2**)$_n$–(**NDI3**)$_n$–(**NDI4**)$_n$ with a redox gradient resulted in even more efficient photocurrent generation (Chart 13).

In addition to NDI, PDI was also applied to the SOSIP protocol.[97] Under similar conditions, a photoactive system of **SOSIP–PDI2** generated a photocurrent 55 times greater than that from **SOSIP–PDI1**. The reason for such significant improvement was attributed to the twisted aromatic core of the substituted PDI, which caused poor π–π stacking and hampered electron transporting, while the unsubstituted PDI had a planar aromatic surface devoid of such problems (Chart 14).

A prominent advantage of the covalently fixed SOSIP system was that it could be post-modified chemically *via* exchange reactions (Fig. 9).[98] For example, porphyrins and phthalocyanines can be integrated into SOSIP NDI polymers using this stack-exchange method to produce double-channel photoactive systems with antiparallel redox gradients.[99] Photocurrents were greatly improved after such modifications, since photo-induced charge separation was highly favored and the charge recombination process was effectively suppressed in the presence of an additional electron donor or acceptor. An even more complex assembly with three coaxial charge-transporting channels was also demonstrated, with NDI stacks in the centre, fullerene stacks as electron transport channels at the periphery, and squaraine stacks as hole channels between the two (Fig. 10).[100] Compared with the double channel systems, the three-channel scaffold afforded further increased photocurrent.

In general, this SOSIP provides a convenient protocol for constructing sophisticated coaxial D–A stacks with a covalent framework. Photo-induced electron transfer and transport were realized with this design. Fundamentally, this method still relied on noncovalent recognition among aromatic molecules (NDI) to achieve spontaneous stacking, prior to covalent coupling. Hence, learning to acquire more power for better control and manipulating noncovalent forces and supramolecular structures at will are again shown to be of vital importance.

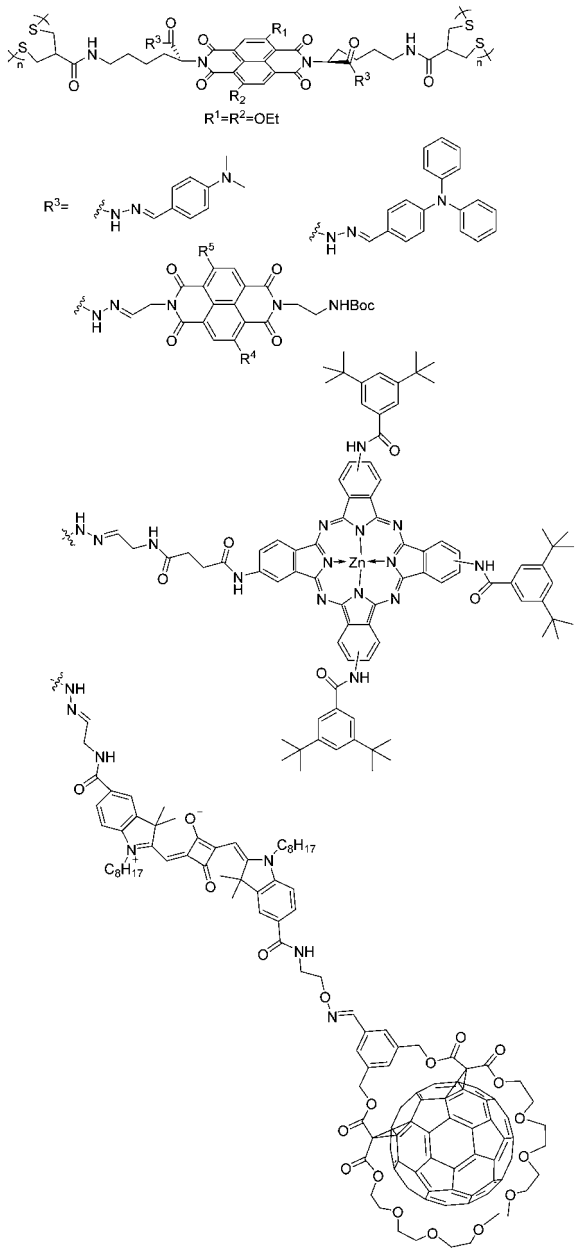

Chart 14 Assemblies generated through post-SOSIP stack-exchange.[98]

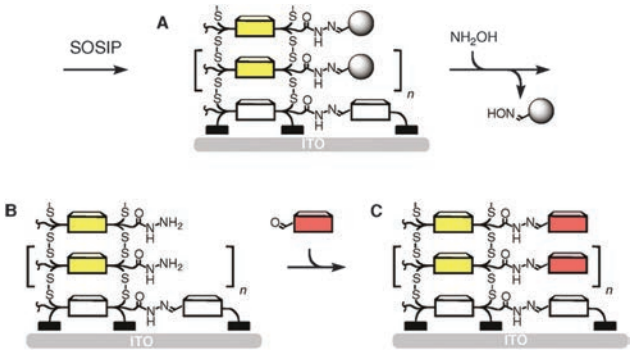

Fig. 9 Illustration of stack exchange for SOSIP-generated assemblies. (Adapted with permission from ref. 98. Copyright (2011) American Chemical Society.)

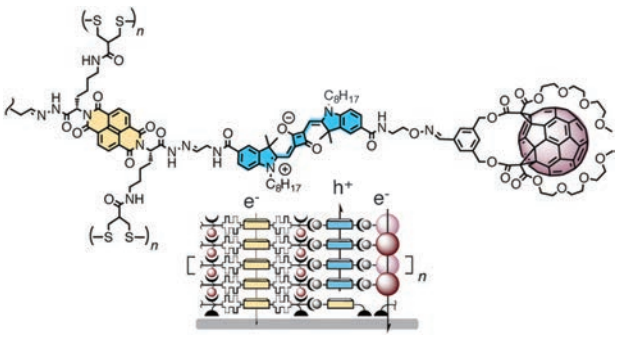

Fig. 10 Illustration of the three-channel assembly of **NDI–Sq-C60**. (Adapted with permission from ref. 100. Copyright (2013) American Chemical Society.)

In summary, from the above systems it is perceivable that various noncovalent forces with different characteristics exert distinct influences over the assembling behaviors and aggregation properties. As shown by the properties summarized in Table 1, the metal–ligand interaction is a relatively powerful noncovalent force and exhibits the most prominent specificity for substrates, *i.e.*, the metal centre and coordinating ligands. With a large free energy release, such interactions allow the assemblies to be readily formed by simply mixing the metal- and ligand-containing partners in solutions. Photo-induced charge separation was achieved with suitable donor and acceptor groups built into the assembly frameworks. However, carrier transport abilities are yet to be realized for such coordinated systems.

In contrast, π–π interactions are a more common type of noncovalent force widely found with almost all different aromatic molecules with large π-surfaces. As a relatively weak noncovalent interaction, it is highly sensitive to the environmental conditions and more than often co-exists with other supramolecular forces such as solvophobic interactions. Accordingly, slow assembly kinetics is usually favourable or even required to achieve highly ordered supramolecular structures dominated by such interactions. The most distinct advantage of π–π stacking is its high compatibility with charge transport, since the face-to-face stacked aromatic surfaces conveniently allow the establishment of π-orbital overlapping and thus facilitate charge transport. This feature readily promotes the π–π stacked molecular aggregates to perform photoconducting and photovoltaic functions. Due to such invaluable properties, π–π interactions are present in almost all molecular assemblies designed for photoconductive and photovoltaic applications. In addition to acting as the sole supramolecular driving force, π–π stacking has also been deployed to work cooperatively and orthogonally with other noncovalent interactions, such as H-bonding, metal–ligand coordination and so on, to form hierarchical supramolecular assemblies. The

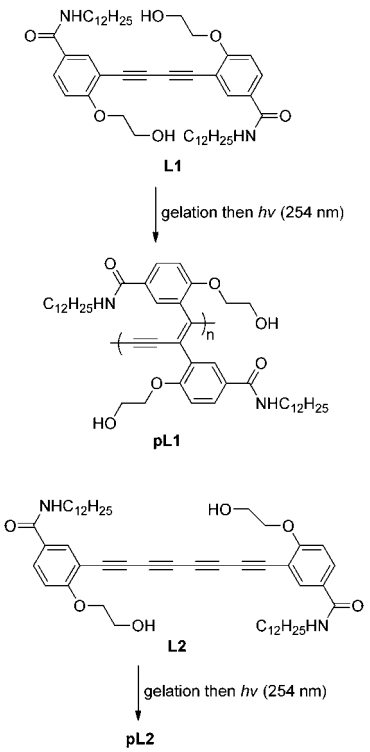

Scheme 2 Polymerizations of acyclic di- and tetraacetylenes.[108–110]

combination of multiple types of noncovalent forces further amplifies the versatility and potency of the self-assembly tactic in creating supramolecular functional systems. Covalent bonds, after all, offer the most stable and reliable molecular scaffolds. Learning from the paradigm of natural systems, noncovalent interaction-facilitated photoactive polymer syntheses are successfully achieved.

In the following part of the review, we will continue to witness the important role of π–π stacking in the generation of molecular assemblies capable of photo-chemical reactions.

3 Photo-induced chemical reactions in molecular aggregates

In this part, we will review a number of intermolecular photochemical reactions that happen uniquely in molecular assemblies. Upon aggregation, monomers are in more intimate contact with one another than in solution. Also, in the aggregated state molecules are confined to a specific intermolecular orientation, which may be different from that in the crystalline or amorphous condensed state. This situation offers unique opportunities to alter the chemical reaction pathways. Examples are introduced below, showing that compared to solution-phased reactions, regio- and/or stereo-selectivity is altered or improved when photochemical reactions happen in molecular aggregates, by virtue of the peculiar intermolecular arrangements facilitated by intermolecular aggregation.[20,21,101,102]

3.1 Photopolymerization of diacetylenes in organogels

Owing to their eminent sensitivity to stimuli, such as temperature and chemical reagents, polydiacetylenes (PDAs) composed of alternating triple and double bonds have been employed as sensory materials.[103–105] However compared to other types of conjugated polymers,[103,105,106] PDA is a much less explored and utilized conjugated polymer structure. One of the important reasons for PDA being less exploited is the difficulty and limited methods available for its preparation. The typical conditions for polymerizing diacetylene molecules involves photoirradiation of monomers in a highly ordered crystalline or liquid crystalline state. Goroff and co-workers have been developing effective methods to prepare various single crystal PDAs.[23] However, high-quality single crystals suitable for conducting solid-state polymerizations are not always accessible. Developing alternative methodologies to prepare PDAs is highly warranted.

Morin and co-workers demonstrated PDA preparation protocols in organogels, which form more easily than highly ordered crystals.[107] The occurrence of organogels typically results from supramolecular polymer network (aggregate) formation in the presence of a suitable solvent. Most organogel formation is driven by intermolecular π–π stacking and/or H-bonding among the monomers. Van der Waals interactions among long aliphatic side chains may also play a role. As mentioned earlier, similar to the ubiquitous presence of π–π stacking with aromatic molecules, H-bonds commonly exist and can be conveniently introduced with a range of functional groups, such as amide, hydroxy, urea and so on.

Morin and co-workers first studied a diphenyldiacetylene derivative bearing amide and hydroxy groups.[108,109] Testing the gelation ability of **L1** in various organic solvents revealed that the hydroxyethoxy chain groups were vital for the gelation process. A control molecule without such substituents had much lower solubility in most organic solvents. In addition to increasing the solubility, the hydroxylethoxy group could form intermolecular H-bonds that helped stabilize the gel. Upon UV irradiation (λ = 254 nm), the monomer polymerized affording **pL1**, with an M_n of 27.9 kD and a polydispersity index of 1.8. In contrast, a solution-cast film of **L1** did not produce polymers under the same irradiation conditions. XRD characterizations confirmed the gel had a more ordered structure than the solution-cast film (Scheme 2).

An analogous molecule **L2** also formed a gel in a variety of organic solvents.[110] The gel from **L2** in chloroform turned into a dark solution after exposure to UV irradiation, while nanofibril structures observed with **L2** turned into nanoparticles of relatively uniform sizes after polymerization (Fig. 11). Polymerized **pL2** exhibited a broad absorption spectrum ranging widely from 300 to 700 nm, but its chemical identity remained inconclusive.

Subsequently, a star shaped monomer **S1** having three diacetylene groups and similar side chains to **L1** was investigated regarding its self-assembly and photo-polymerization abilities.[111] Monomer **S1** formed gels in DMSO and aromatic

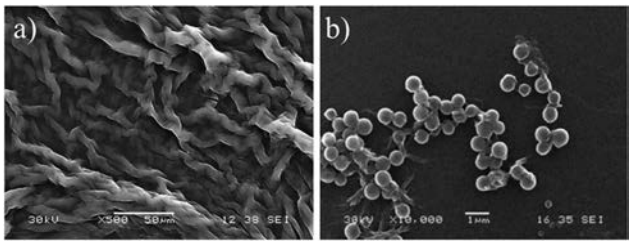

Fig. 11 SEM images of **L2** (a) and **pL2** (b). (Reproduced from ref. 110 with permission from The Royal Society of Chemistry.)

solvents. XRD identified a small π–π stacking distance of 0.33 nm in the gel, along with an inter-columnar distance slightly smaller than the length of the molecular arms, suggesting partial interdigitation of the alkyl chains (Scheme 3). Varied-temperature NMR spectra of **S1** in DMSO-d_6 confirmed the presence of H-bonds between the amide groups and occurrence of π–π stacking between the aromatic skeleton (Fig. 12). The xerogel from **S1** in toluene could also be polymerized upon UV irradiation, giving a dark-blue film containing nano-wired PDA of **pS1** (Fig. 13).

The authors further studied the gelation properties of a series of phenyleneethynylene macrocycles, all of which had amide groups in the side chain and were thus capable of intermolecular H-bonding.[112] Evidently, π–π stacking

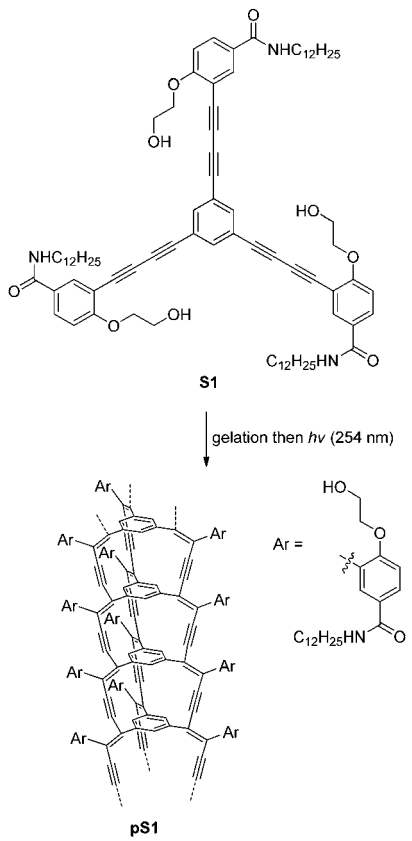

Scheme 3 Polymerization of a star-shaped diacetylene molecule.[111]

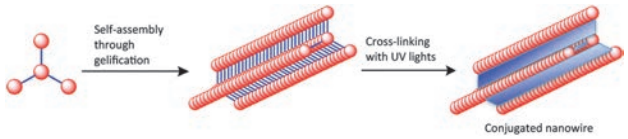

Fig. 12 Illustrative models of **S1**, the **S1** aggregate and **pS1**. (Reproduced with permission from ref. 111. Copyright © 2013, American Chemical Society.)

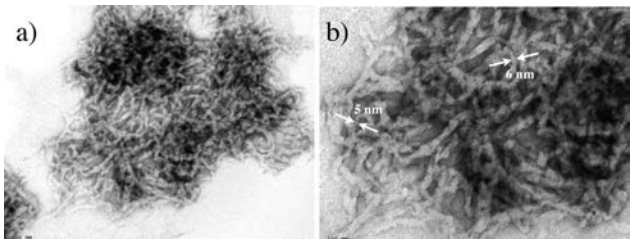

Fig. 13 TEM images of **pS1** dispersed in methanol (scale bars are (a) 200 nm and (b) 100 nm). (Reprinted with permission from ref. 111. Copyright © 2013, American Chemical Society.)

interactions among these macrocycles having unsaturated backbones were inevitable given suitable solvent conditions. It was found that **MC1** exhibited intermolecular H-bonds between the amide groups, very good gelation ability, as well as relatively ordered structures in the gel state, as evidenced by XRD. In contrast, **MC2** had a much better solubility but lower gelation ability. Besides the fact that urethane is a weaker H-bonding moiety than the amide group, presumably a more flexible linkage between the macrocycle backbone and H-bonding unit was an important reason for the lower gelation ability of **MC2** (Chart 15).

Nonetheless, in spite of its evident gelling ability, **MC1** displayed very low photo-reactivity and was not suitable for photo-polymerization. As a modified analogue of **MC1**, **MC3** was designed. In addition to a potent H-bonding amide group, a more reactive diacetylene moiety was introduced to the side chains, as it was decoupled from the macrocycle backbone.[114] **MC3** formed a gel in various organic solvents, and the gel with ethyl acetate was very reactive even under ambient conditions, since it turned blue rapidly upon UV irradiation, indicating the formation of PDA. Soluble nanorods resulted from this photo-polymerization reaction. The XRD pattern confirmed an ordered columnar packing of **MC3** in the gel state. Impressively, Raman spectroscopy conducted for **MC3** and the purified nanorods revealed that the diacetylene units in the cyclic backbone were also polymerized under UV light. The reason for this result was proposed as follows. After the polymerization of diacetylene units in the side chains, the diacetylene groups in the macrocycle backbone became spatially closer to one another and hence more ready to react photochemically.

In order to investigate the effect of amide configuration on the self-aggregation behaviors and photo-reactivity of the macrocycles, **MC4–5** were then prepared and compared to

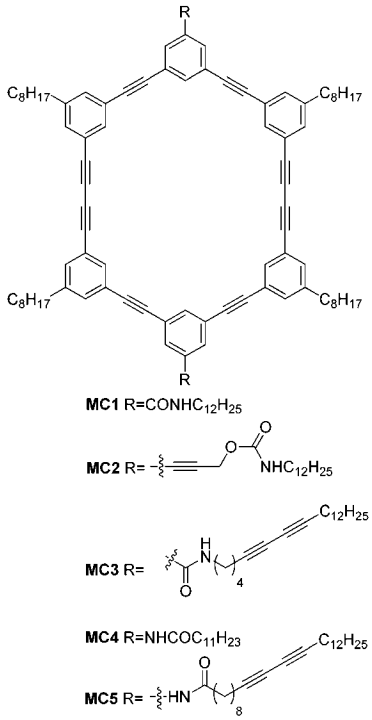

Chart 15 Chemical structures of macrocycles containing diacetylene groups.[112–114]

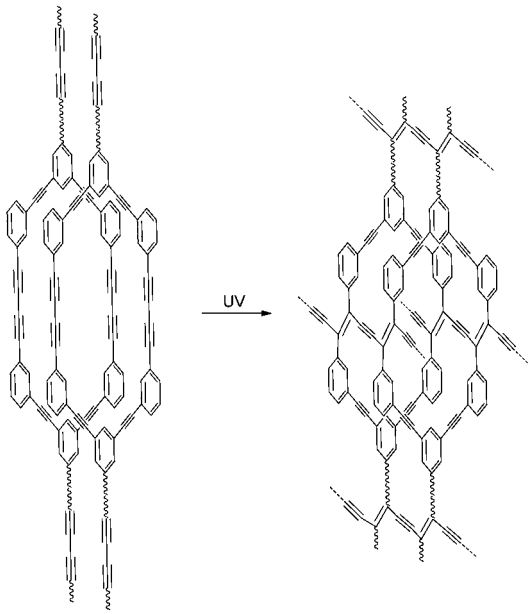

Scheme 4 Structures of PDA nanorod from **MC3**.

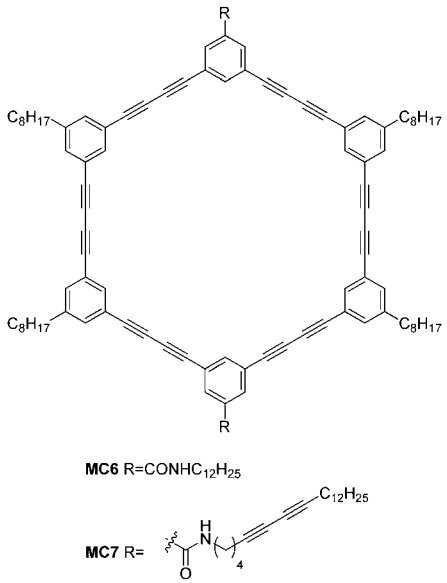

Chart 16 Chemical structures of phenylene diacetylene macrocycles with diacetylene side chains.[115]

MC1 and **MC3**.[113] MALDI-TOF mass spectroscopy was able to detect aggregates up to hexamers for all four macrocycles. However, in contrast to **MC1** and **MC3** which were good gelators, **MC4–5** exhibited poor gelation abilities. Upon UV irradiation, the gels from **MC4–5** exhibited a color change and turned orange, along with a significant loss in gel viscosity, suggesting that partial decomposition had occurred (Scheme 4). DFT calculations confirmed the experimental results by showing that the molecular orientation of the benzamide macrocycles (**MC1** and **MC3**) in the aggregated state was more compatible with the photo-polymerization process, thus leading to higher photo-reactivity (Chart 16).

MC6–7 having six cyclic diacetylene groups were then designed as precursors to stronger nanotubes upheld by six PDA chains.[115] Being not particularly good gelators, **MC6–7** formed translucent gels only in cyclohexane, featuring columnar packed macrocycles. Moreover, unlike **MC3** with which topochemical polymerization was facilitated by the diacetylene groups in the side chains, **MC7** bearing diacetylenes in the side chains only underwent a partial polymerization. Impressively, high photo-reactivity was observed with gels of **MC6** without the side-chain diacetylene units. The resultant nanotube from **MC6** could be visualized with HRTEM owing to its robust structure consisting of six PDA chains.

3.2 Cycloaddition of molecules with cation–π interactions

The strength of π–π interactions is related to the surface area and planarity of aromatic frameworks. Normally, small aromatic rings like benzene do not confer adequate π–π interactions. Moreover, π–π interactions do not have a very specific direction or orientation. Slipped and rotated packing motifs are often observed. Cation–π interactions are a stronger noncovalent force that may occur between positively charged arene and electron-rich aromatic rings. As they also involve the stacking of two aromatic moieties, with suitable substrates they may be used to reinforce π–π stacking interactions. Additionally, they confer better directionality for aromatic stacking. In this part, we review a couple of photo-induced cycloaddition reactions of a set of olefin substrates under the influence of

cation–π interactions. Improved regio- and stereo-selectivity was attained by virtue of the more favorable intermolecular orientation in the aggregates.

Yamada and co-workers successfully exploited cation–π interactions between arene and cationic azaarene to bridge the distance between two olefin units and achieved a desirable orientation. Therefore higher regio- and stereo-selectivities were realized with the photo-cycloaddition reaction. The first reported example was the dimerization of *trans*-4-styrylpyridines.[116] Under neutral conditions, UV irradiation of compound **E1a** in a methanol solution gave a mixture of [2+2] cycloaddition products including **E12a**, **E13a** and **E14a**, as well as the isomerization product **E16a**. Continuously increasing the amount of HCl up to 10 equivalents in solution was found to selectively raise the yield of **E12a** up to 71%, while at the same time the isomerization product **E16a** was effectively suppressed to 8%. Adding an electron-donating methoxy group to the phenyl ring of **E1c** had a favorable effect on the reaction selectivity, as the yield of **E12c** reached 95% in the presence of only 3 eq. of HCl. On the other hand, with substrate **E1b** bearing an electron-withdrawing trifluoromethyl group a decreased yield of 27% was observed under the same conditions. Such electronic effects suggested that the intermolecular association of **E1a** under acidic conditions, induced by a cation–π interaction, was likely the cause of the altered selectivity of the reactions. This conclusion was supported by the single crystal structures of **E1a** and **E1a**·HCl (Fig. 14). The crystal structure of pure **E1a** showed separated and edge-to-face orientations of the phenyl and pyridine rings, while that of **E1a**·HCl contained an ordered, alternating stacking motif of pyridinium and phenyl rings, with a face-to-face distance of only 0.33 nm. **E1a**·HCl could also be converted to **E12a** in a high yield within the single crystals under UV irradiation.

Subsequently, cucurbit[8]uril was used to assist the cation–π interaction between the pyridinium ion and phenyl units. In a dilute aqueous solution, the photo-irradiation of **E1a**·HCl only afforded isomer **E16a**. Upon the addition of 0.5 eq. of cucurbit[8]uril, the yield of dimer **E12a** was improved to 62%. However, under the same conditions, the major product from

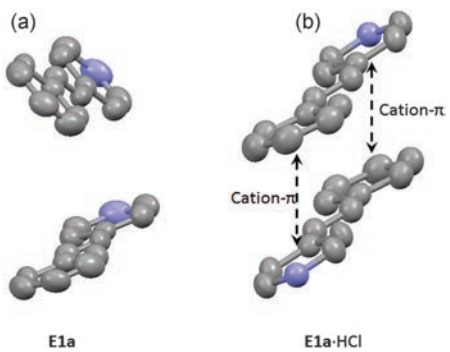

Fig. 14 Single crystal structures of **E1a** (a) and **E1a**·HCl (b). (Thermal ellipsoid at 50%, hydrogen atoms and HCl molecules are omitted for clarity. Produced from .cif files reported from ref. 116. Copyright © 2007, American Chemical Society.)

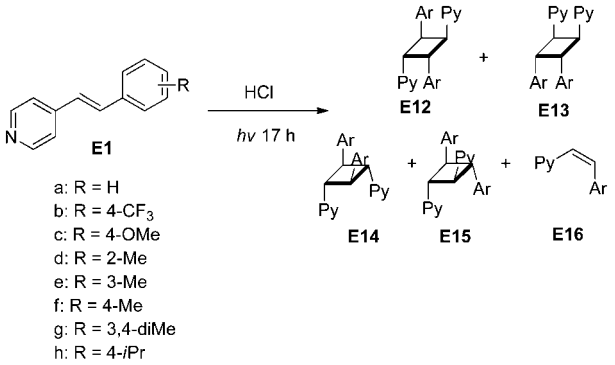

Scheme 5 [2+2] cycloaddition of *trans*-4-styrylpyridine derivatives.[116,117]

the photo-reactions of the substrates **E1d**, **E1e**, and **E1g** was the head-to-head dimer **E13**. These results were attributed to the steric hindrance caused by 2/3-methyl groups, which impeded the complexing of these substrates with cucurbit[8]uril. Instead, product **E12** could be acquired in acidified methanol for these three substrates, where the steric hindrance was not a particular issue. When the substitute (methyl or isopropyl) was located on carbon 4, as in **E1f** and **E1h**, steric hindrance did not seem to affect the inclusion of these substrates by cucurbit[8]uril. **E12f** and **E12h** were obtained with the assistance of a cucurbit[8]uril host in the presence of HCl (Scheme 5).[117]

The same type of supramolecular interaction has also been studied with the photo-induced dimerization of 4-azachalcone derivatives **E2**, but only in the solid state.[118] The head-to-tail products **E22** were obtained quantitatively upon irradiating both substrates **E2a** and **b** in the pyridium form. Even though the substrates existed in the neutral form in crystals, exposure of the crystals to HCl(*g*) induced a re-orientation of the molecules in the crystalline state (Scheme 6).[119] Upon UV irradiation, the head-to-tail dimer **E22** was acquired (Fig. 15).

The selective head-to-tail photo-dimerization of protonated phenylvinylpyridine and naphthylvinylpyridine was successfully carried out with crystals in the presence of water.[120] In the absence of water or HCl, the reactions could not take place (Scheme 7).

Cation–π interactions were also employed to modulate the [4+4] photo-dimerization of azaanthracenes.[121] Upon photo-irradiation, azaanthracene **E4** was selectively transformed into the head-to-tail *anti*-dimer **E42** (95%) under acidic conditions (3 eq. HCl) in methanol, although a relatively high concentration

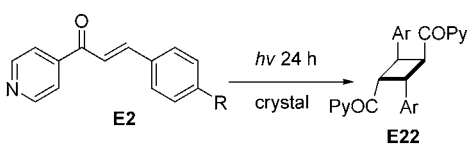

Scheme 6 [2+2] cycloaddition of *trans*-3-phenyl-1-pyridylpropenone derivatives.[118]

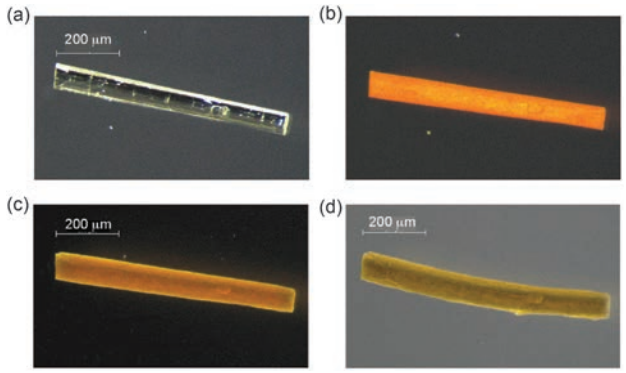

Fig. 15 Photomicrographs of a single crystal of **E2b** before (a) and after exposure to HCl gas for 10 s (b) and (c) for 10 min, and (d) after irradiation of the resultant HCl salt. (Reproduced from ref. 119 with permission from The Royal Society of Chemistry.)

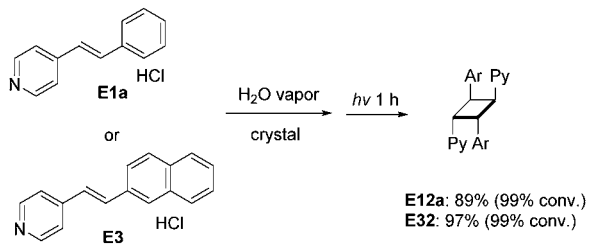

Scheme 7 [2+2] cycloaddition of *trans*-4-styrylpyridine derivatives.[120]

(1.0 M) of substrate was required. This reaction could also be carried out in crystals in the presence of HCl, but no reaction occurred in the absence of HCl. Another azaanthracene **E5** was found to have a similar reactivity, favored by the cation–π interaction (Scheme 8).

In summary of this section, molecular aggregation provides a viable method for attaining intermolecular photochemical reactions in solution. Unique or improved selectivities can even be attained by virtue of the intimate molecular contact and particular reactive group orientations in such supramolecular assemblies. Aromatic stacking and solvophobic interactions are among the most commonly and conveniently employed supramolecular forces to assemble relevant aggregates. The above systems also demonstrate that simultaneously employing other types of noncovalent forces, such as H-bonding and cation–π interactions to compliment π–π and solvophobic interactions can effectively circumvent their drawback of lacking specific directionality, and strengthened intermolecular aggregation can also be obtained.

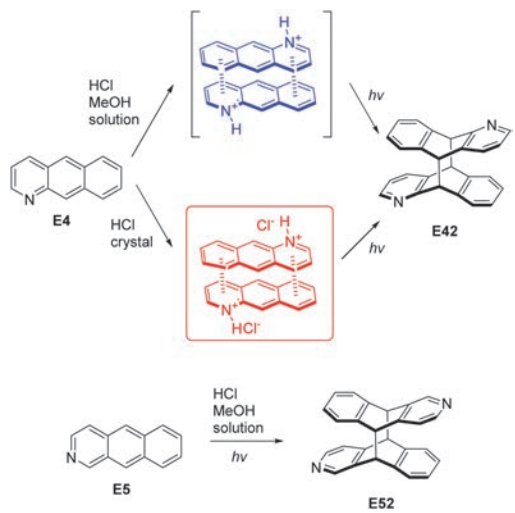

Scheme 8 [4+4] cycloadditions of azaanthracene substrates.[121]

4 Summary

Appropriate supramolecular organization can exert favorable effects on the photochemical processes that happen within their frameworks. Particularly, photo-induced electron transfer can be facilitated by stabilizing separated charges among aggregated carrier hosts, and charge transport can be realized if carrier transporting channels are suitably formed in the assembly architectures. On the other hand, special reaction selectivity in photochemical transformations is also achievable given that proper intermolecular orientations are afforded by supramolecular aggregates. In view of these important consequences, the rational design and successful creation of supramolecular systems with specific structures and properties are highly desirable. To fulfill such goals, the abilities to precisely control and fine-tune the noncovalent interactions that dictate supramolecular assemblies are required, which necessarily entails a thorough understanding of these supramolecular forces.

From literature reports, it is perceivable that the great diversity of various noncovalent forces greatly facilitates their application in supramolecular architectures. Although the strength of individual supramolecular interactions is typically weak, the collective force among a large number of molecules can be very significant, capable of realizing supramolecular structures with adequate stabilities and accomplishing photochemical functions. Moreover, the facile formation and reversibility of these noncovalent bonds uniquely offer a self-assembly approach. At the moment there is no other technique that can compete and outperform self-assembly in its efficiency and precision at manipulating and arranging molecules within nanoscale dimensions. Hence, noncovalent forces and self-assembly are indispensable tools for building complex hierarchical supramolecular systems to perform sophisticated functions.

Certain types of noncovalent interactions, *e.g.*, π–π stacking, H-bonding, solvophobic effects and metal–ligand coordination, are used more frequently than others in building supramolecular systems to fulfill charge transport and photochemical reactions. In particular, π–π interactions are one of the most popularly applied noncovalent tools, not only due to their ubiquitous existence with aromatic molecules, but also for a number of their unrivaled merits. The strength of π–π stacking

can be readily and sensitively tuned by varying the size, electronic and steric features of aromatic frameworks. Even more importantly, the close contacts between aromatic moieties brought about by π–π interactions conveniently enable effective orbital overlapping and thus charge transporting ability. Short distances between reactive groups in aggregated molecules are also important for photochemical reactions to occur. Furthermore, π–π stacking interactions can be conveniently designed to work cooperatively with other noncovalent forces, including solvophobic, H-bonding, and metal–ligand interactions, in creating hierarchical systems.

The versatility and values of noncovalent interactions are also presented by employing them to compliment covalent bonds in constructing large covalent functional architectures. While nature illustrates the perfect paradigms of seamlessly combined uses of covalent and noncovalent bonds with templated syntheses of nucleic acids and proteins, similar strategies have been smartly emulated in synthetic systems, including in assembling macromolecular photoactive objects.

By reviewing the above systems, particularly summarizing the chemical characteristics and assembling tactics executed in the accomplished work, certain design guidelines are hopefully outlined, useful and applicable to the future development of more complex supramolecular systems with more advanced functions.

Acknowledgements

The work is supported by the National Natural Science Foundation of China (Projects 21174004, 21222403, 51073002 and 21074004) and the Ministry of Science and Technology (2011CB606106 and 2012CB933501).

Notes and references

1 T. Aida, E. W. Meijer and S. I. Stupp, *Science*, 2012, **335**, 813–817.
2 G. McDermott, S. Prince, A. Freer, A. Hawthornthwaite-Lawless, M. Papiz, R. Cogdell and N. Isaacs, *Nature*, 1995, **374**, 517–521.
3 R. J. Cogdell, A. Gall and J. Köhler, *Q. Rev. Biophys.*, 2006, **39**, 227–324.
4 M. Grätzel, *Acc. Chem. Res.*, 1981, **14**, 376–384.
5 M. R. Wasielewski, *Chem. Rev.*, 1992, **92**, 435–461.
6 L. Sun, L. Hammarstrom, B. Akermark and S. Styring, *Chem. Soc. Rev.*, 2001, **30**, 36–49.
7 J. H. Alstrum-Acevedo, M. K. Brennaman and T. J. Meyer, *Inorg. Chem.*, 2005, **44**, 6802–6827.
8 A. C. Benniston and A. Harriman, *Mater. Today*, 2008, **11**, 26–34.
9 C.-C. Chu and D. M. Bassani, *Photochem. Photobiol. Sci.*, 2008, **7**, 521–530.
10 D. Gust, T. A. Moore and A. L. Moore, *Acc. Chem. Res.*, 2009, **42**, 1890–1898.
11 K. Kalyanasundaram and M. Grätzel, *Curr. Opin. Biotechnol.*, 2010, **21**, 298–310.
12 E. S. Andreiadis, M. Chavarot-Kerlidou, M. Fontecave and V. Artero, *Photochem. Photobiol.*, 2011, **87**, 946–964.
13 H. Zhou, T. Fan and D. Zhang, *ChemCatChem*, 2011, **3**, 513–528.
14 G. D. Scholes, G. R. Fleming, A. Olaya-Castro and R. van Grondelle, *Nat. Chem.*, 2011, **3**, 763–774.
15 M. Carraro, A. Sartorel, F. M. Toma, F. Puntoriero, F. Scandola, S. Campagna, M. Prato and M. Bonchio, in *Photocatalysis*, ed. C. A. Bignozzi, 2011, vol. 303, pp. 121–150.
16 Y. Tachibana, L. Vayssieres and J. R. Durrant, *Nat. Photonics*, 2012, **6**, 511–518.
17 M. D. Kärkäs, E. V. Johnston, O. Verho and B. Åkermark, *Acc. Chem. Res.*, 2013. Q7
18 M. R. Wasielewski, *Acc. Chem. Res.*, 2009, **42**, 1910–1921.
19 P. D. Frischmann, K. Mahata and F. Würthner, *Chem. Soc. Rev.*, 2013, **42**, 1847–1870.
20 H. Bouas-Laurent, A. Castellan, J.-P. Desvergne and R. Lapouyade, *Chem. Soc. Rev.*, 2000, **29**, 43–55.
21 H. Bouas-Laurent, A. Castellan, J.-P. Desvergne and R. Lapouyade, *Chem. Soc. Rev.*, 2001, **30**, 248–263.
22 G. Kaupp, *J. Phys. Org. Chem.*, 2008, **21**, 630–643.
23 J. W. Lauher, F. W. Fowler and N. S. Goroff, *Acc. Chem. Res.*, 2008, **41**, 1215–1229.
24 K. Biradha and R. Santra, *Chem. Soc. Rev.*, 2013, **42**, 950–967.
25 R. Bhosale, J. Misek, N. Sakai and S. Matile, *Chem. Soc. Rev.*, 2010, **39**, 138–149.
26 S. Matile, A. V. Jentzsch, J. Montenegro and A. Fin, *Chem. Soc. Rev.*, 2011, **40**, 2453–2474.
27 S. Fukuzumi, T. Honda and T. Kojima, *Coord. Chem. Rev.*, 2012, **256**, 2488–2502.
28 S. Hecht, *Small*, 2005, **1**, 26–29.
29 S. Yagai, T. Karatsu and A. Kitamura, *Chem.–Eur. J.*, 2005, **11**, 4054–4063.
30 S. Yagai and A. Kitamura, *Chem. Soc. Rev.*, 2008, **37**, 1520–1529.
31 M.-M. Russew and S. Hecht, *Adv. Mater.*, 2010, **22**, 3348–3360.
32 A. Ajayaghosh and V. K. Praveen, *Acc. Chem. Res.*, 2007, **40**, 644–656.
33 M. B. Smith and J. Michl, *Chem. Rev.*, 2010, **110**, 6891–6936.
34 R. N. Dsouza, U. Pischel and W. M. Nau, *Chem. Rev.*, 2011, **111**, 7941–7980.
35 Y. Hong, J. W. Y. Lam and B. Z. Tang, *Chem. Soc. Rev.*, 2011, **40**, 5361–5388.
36 G. de la Torre, G. Bottari, M. Sekita, A. Hausmann, D. M. Guldi and T. Torres, *Chem. Soc. Rev.*, 2013, **42**, 8049–8105.
37 C.-H. Huang and D. M. Bassani, *Eur. J. Org. Chem.*, 2005, 4041–4050.
38 Y. Inokuma, M. Kawano and M. Fujita, *Nat. Chem.*, 2011, **3**, 349–358.

39 T. Lei and J. Pei, *J. Mater. Chem.*, 2012, **22**, 785–798.
40 H. Dong, H. Zhu, Q. Meng, X. Gong and W. Hu, *Chem. Soc. Rev.*, 2012, **41**, 1754–1808.
41 H. Imahori and T. Umeyama, *J. Phys. Chem. C*, 2009, **113**, 9029–9039.
42 J. Elemans, R. Van Hameren, R. J. M. Nolte and A. E. Rowan, *Adv. Mater.*, 2006, **18**, 1251–1266.
43 C. M. Drain, A. Varotto and I. Radivojevic, *Chem. Rev.*, 2009, **109**, 1630–1658.
44 B. Rybtchinski, *ACS Nano*, 2011, **5**, 6791–6818.
45 M. K. Panda, K. Ladomenou and A. G. Coutsolelos, *Coord. Chem. Rev.*, 2012, **256**, 2601–2627.
46 Y. N. Teo and E. T. Kool, *Chem. Rev.*, 2012, **112**, 4221–4245.
47 F. Würthner, T. E. Kaiser and C. R. Saha-Moller, *Angew. Chem., Int. Ed.*, 2011, **50**, 3376–3410.
48 J. W. Steed, D. R. Turner and K. J. Wallace, *Core concepts in supramolecular chemistry and nanochemistry*, Wiley, 2007.
49 S. Ehrlich, J. Moellmann and S. Grimme, *Acc. Chem. Res.*, 2012, **46**, 916–926.
50 L. M. Salonen, M. Ellermann and F. Diederich, *Angew. Chem., Int. Ed.*, 2011, **50**, 4808–4842.
51 T. F. De Greef, M. M. Smulders, M. Wolffs, A. P. Schenning, R. P. Sijbesma and E. Meijer, *Chem. Rev.*, 2009, **109**, 5687–5754.
52 X. Zhao and Z.-T. Li, *Chem. Commun.*, 2010, **46**, 1601–1616.
53 C. J. Pedersen, *J. Am. Chem. Soc.*, 1967, **89**, 7017–7036.
54 G. Kumar and R. Gupta, *Chem. Soc. Rev.*, 2013.
55 F. D'Souza and O. Ito, *Chem. Commun.*, 2009, 4913–4928.
56 F. D'Souza, N. P. Rath, G. R. Deviprasad and M. E. Zandler, *Chem. Commun.*, 2001, 267–268.
57 F. D'Souza, G. R. Deviprasad, M. E. Zandler, M. E. El-Khouly, M. Fujitsuka and O. Ito, *J. Phys. Chem. A*, 2003, **107**, 4801–4807.
58 M. E. El-Khouly, L. M. Rogers, M. E. Zandler, G. Suresh, M. Fujitsuka, O. Ito and F. D'Souza, *ChemPhysChem*, 2003, **4**, 474–481.
59 F. D'Souza, S. Gadde, M. E. Zandler, M. Itou, Y. Araki and O. Ito, *Chem. Commun.*, 2004, 2276–2277.
60 S. Fukuzumi, K. Saito, K. Ohkubo, T. Khoury, Y. Kashiwagi, M. A. Absalom, S. Gadde, F. D'Souza, Y. Araki, O. Ito and M. J. Crossley, *Chem. Commun.*, 2011, **47**, 7980–7982.
61 C. She, S. J. Lee, J. E. McGarrah, J. Vura-Weis, M. R. Wasielewski, H. Chen, G. C. Schatz, M. A. Ratner and J. T. Hupp, *Chem. Commun.*, 2010, **46**, 547–549.
62 W. Pisula, A. Menon, M. Stepputat, I. Lieberwirth, U. Kolb, A. Tracz, H. Sirringhaus, T. Pakula and K. Müllen, *Adv. Mater.*, 2005, **17**, 684–689.
63 L. Schmidt-Mende, A. Fechtenkotter, K. Mullen, E. Moons, R. H. Friend and J. D. MacKenzie, *Science*, 2001, **293**, 1119–1122.
64 J. P. Hill, W. Jin, A. Kosaka, T. Fukushima, H. Ichihara, T. Shimomura, K. Ito, T. Hashizume, N. Ishii and T. Aida, *Science*, 2004, **304**, 1481–1483.
65 W. Jin, Y. Yamamoto, T. Fukushima, N. Ishii, J. Kim, K. Kato, M. Takata and T. Aida, *J. Am. Chem. Soc.*, 2008, **130**, 9434–9440.
66 Y. Yamamoto, T. Fukushima, Y. Suna, N. Ishii, A. Saeki, S. Seki, S. Tagawa, M. Taniguchi, T. Kawai and T. Aida, *Science*, 2006, **314**, 1761–1764.
67 Y. He, Y. Yamamoto, W. Jin, T. Fukushima, A. Saeki, S. Seki, N. Ishii and T. Aida, *Adv. Mater.*, 2010, **22**, 829–832.
68 Y. Yamamoto, G. Zhang, W. Jin, T. Fukushima, N. Ishii, A. Saeki, S. Seki, S. Tagawa, T. Minari, K. Tsukagoshi and T. Aida, *Proc. Natl. Acad. Sci. U. S. A.*, 2009, **106**, 21051–21056.
69 W.-S. Li, Y. Yamamoto, T. Fukushima, A. Saeki, S. Seki, S. Tagawa, H. Masunaga, S. Sasaki, M. Takata and T. Aida, *J. Am. Chem. Soc.*, 2008, **130**, 8886–8887.
70 R. Charvet, D.-L. Jiang and T. Aida, *Chem. Commun.*, 2004, 2664–2665.
71 R. Charvet, Y. Yamamoto, T. Sasaki, J. Kim, K. Kato, M. Takata, A. Saeki, S. Seki and T. Aida, *J. Am. Chem. Soc.*, 2012, **134**, 2524–2527.
72 Y. Hizume, K. Tashiro, R. Charvet, Y. Yamamoto, A. Saeki, S. Seki and T. Aida, *J. Am. Chem. Soc.*, 2010, **132**, 6628–6629.
73 W.-S. Li, A. Saeki, Y. Yamamoto, T. Fukushima, S. Seki, N. Ishii, K. Kato, M. Takata and T. Aida, *Chem.–Asian J.*, 2010, **5**, 1566–1572.
74 H. Langhals, *Helv. Chim. Acta*, 2005, **88**, 1309–1343.
75 S. E. Wheeler, *Acc. Chem. Res.*, 2012, **46**, 1029–1038.
76 M. M. Safont-Sempere, G. Fernández and F. Würthner, *Chem. Rev.*, 2011, **111**, 5784–5814.
77 H. Shao, M. Gao, S. H. Kim, C. P. Jaroniec and J. R. Parquette, *Chem.–Eur. J.*, 2011, **17**, 12882–12885.
78 H. Shao, T. Nguyen, N. C. Romano, D. A. Modarelli and J. R. Parquette, *J. Am. Chem. Soc.*, 2009, **131**, 16374–16376.
79 H. Shao and J. R. Parquette, *Chem. Commun.*, 2010, **46**, 4285–4287.
80 H. Shao, J. Seifert, N. C. Romano, M. Gao, J. J. Helmus, C. P. Jaroniec, D. A. Modarelli and J. R. Parquette, *Angew. Chem., Int. Ed.*, 2010, **49**, 7688–7691.
81 S. Tu, S. H. Kim, J. Joseph, D. A. Modarelli and J. R. Parquette, *J. Am. Chem. Soc.*, 2011, **133**, 19125–19130.
82 A. P. H. J. Schenning, J. v. Herrikhuyzen, P. Jonkheijm, Z. Chen, F. Würthner and E. W. Meijer, *J. Am. Chem. Soc.*, 2002, **124**, 10252–10253.
83 F. Würthner, Z. Chen, F. J. M. Hoeben, P. Osswald, C.-C. You, P. Jonkheijm, J. v. Herrikhuyzen, A. P. H. J. Schenning, P. P. A. M. van der Schoot, E. W. Meijer, E. H. A. Beckers, S. C. J. Meskers and R. A. J. Janssen, *J. Am. Chem. Soc.*, 2004, **126**, 10611–10618.
84 P. Jonkheijm, N. Stutzmann, Z. Chen, D. M. de Leeuw, E. W. Meijer, A. P. H. J. Schenning and F. Würthner, *J. Am. Chem. Soc.*, 2006, **128**, 9535–9540.
85 S. Sengupta and F. Würthner, *Acc. Chem. Res.*, 2013, **46**, 2498–2512.
86 V. Huber, M. Katterle, M. Lysetska and F. Würthner, *Angew. Chem., Int. Ed.*, 2005, **44**, 3147–3151.
87 C. Röger, Y. Miloslavina, D. Brunner, A. R. Holzwarth and F. Würthner, *J. Am. Chem. Soc.*, 2008, **130**, 5929–5939.

88 S. Sengupta, D. Ebeling, S. Patwardhan, X. Zhang, H. von Berlepsch, C. Böttcher, V. Stepanenko, S. Uemura, C. Hentschel, H. Fuchs, F. C. Grozema, L. D. A. Siebbeles, A. R. Holzwarth, L. Chi and F. Würthner, *Angew. Chem., Int. Ed.*, 2012, **51**, 6378–6382.

89 C. Röger, M. G. Müller, M. Lysetska, Y. Miloslavina, A. R. Holzwarth and F. Würthner, *J. Am. Chem. Soc.*, 2006, **128**, 6542–6543.

90 Z. J. Gartner, B. N. Tse, R. Grubina, J. B. Doyon, T. M. Snyder and D. R. Liu, *Science*, 2004, **305**, 1601–1605.

91 X. Li and D. R. Liu, *Angew. Chem., Int. Ed.*, 2004, **43**, 4848–4870.

92 R. S. K. Kishore, O. Kel, N. Banerji, D. Emery, G. Bollot, J. Mareda, A. Gomez-Casado, P. Jonkheijm, J. Huskens, P. Maroni, M. Borkovec, E. Vauthey, N. Sakai and S. Matile, *J. Am. Chem. Soc.*, 2009, **131**, 11106–11116.

93 N. Sakai, A. L. Sisson, T. Buergi and S. Matile, *J. Am. Chem. Soc.*, 2007, **129**, 15758–15759.

94 A. L. Sisson, N. Sakai, N. Banerji, A. Fuerstenberg, E. Vauthey and S. Matile, *Angew. Chem., Int. Ed.*, 2008, **47**, 3727–3729.

95 R. Bhosale, A. Perez-Velasco, V. Ravikumar, R. S. K. Kishore, O. Kel, A. Gomez-Casado, P. Jonkheijm, J. Huskens, P. Maroni, M. Borkovec, T. Sawada, E. Vauthey, N. Sakai and S. Matile, *Angew. Chem., Int. Ed.*, 2009, **48**, 6461–6464.

96 N. Sakai, M. Lista, O. Kel, S.-i. Sakurai, D. Emery, J. Mareda, E. Vauthey and S. Matile, *J. Am. Chem. Soc.*, 2011, **133**, 15224–15227.

97 P. Charbonnaz, N. Sakai and S. Matile, *Chem. Sci.*, 2012, **3**, 1492–1496.

98 N. Sakai and S. Matile, *J. Am. Chem. Soc.*, 2011, **133**, 18542–18545.

99 G. Sforazzini, R. Turdean, N. Sakai and S. Matile, *Chem. Sci.*, 2013, **4**, 1847–1851.

100 G. Sforazzini, E. Orentas, A. Bolag, N. Sakai and S. Matile, *J. Am. Chem. Soc.*, 2013, **135**, 12082–12090.

101 H. Hopf, C. Beck, J.-P. Desvergne, H. Bouas-Laurent, P. G. Jones and L. Ernst, *Beilstein J. Org. Chem.*, 2009, **5**, DOI: 10.3762/bjoc.5.20.

102 J. Reichwagen, H. Hopf, A. Del Guerzo, J. P. Desvergne and H. Bouas-Laurent, *Org. Lett.*, 2004, **6**, 1899–1902.

103 O. Yarimaga, J. Jaworski, B. Yoon and J.-M. Kim, *Chem. Commun.*, 2012, **48**, 2469–2485.

104 X. M. Sun, T. Chen, S. Q. Huang, L. Li and H. S. Peng, *Chem. Soc. Rev.*, 2010, **39**, 4244–4257.

105 B. Yoon, S. Lee and J.-M. Kim, *Chem. Soc. Rev.*, 2009, **38**, 1958–1968.

106 D. J. Ahn, S. Lee and J.-M. Kim, *Adv. Funct. Mater.*, 2009, **19**, 1483–1496.

107 J.-F. Morin, *Synlett*, 2013, **24**, 2032–2044.

108 S. Rondeau-Gagné and J.-F. Morin, *Chem. Soc. Rev.*, 2014, **43**, 85.

109 J. R. Néabo, K. I. S. Tohoundjona and J.-F. Morin, *Org. Lett.*, 2011, **13**, 1358–1361.

110 J. R. Néabo, C. Vigier-Carriere, S. Rondeau-Gagne and J.-F. Morin, *Chem. Commun.*, 2012, **48**, 10144–10146.

111 J. R. Néabo, S. Rondeau-Gagné, C. Vigier-Carrière and J.-F. Morin, *Langmuir*, 2013, **29**, 3446–3452.

112 K. Cantin, S. Rondeau-Gagné, J. R. Neabo, M. Daigle and J.-F. Morin, *Org. Biomol. Chem.*, 2011, **9**, 4440–4443.

113 S. Rondeau-Gagné, J. R. Neabo, M. Desroches, K. Cantin, A. Soldera and J.-F. Morin, *J. Mater. Chem. C*, 2013, **1**, 2680–2687.

114 S. Rondeau-Gagné, J. R. Néabo, M. Desroches, J. Larouche, J. Brisson and J.-F. Morin, *J. Am. Chem. Soc.*, 2012, **135**, 110–113.

115 S. Rondeau-Gagné, J. R. Néabo, M. Desroches, I. Levesque, M. Daigle, K. Cantin and J.-F. Morin, *Chem. Commun.*, 2013.

116 S. Yamada, N. Uematsu and K. Yamashita, *J. Am. Chem. Soc.*, 2007, **129**, 12100–12101.

117 A. Nakamura, H. Irie, S. Hara, M. Sugawara and S. Yamada, *Photochem. Photobiol. Sci.*, 2011, **10**, 1496–1500.

118 S. Yamada and Y. Tokugawa, *J. Am. Chem. Soc.*, 2009, **131**, 2098–2099.

119 S. Yamada, Y. Tokugawa, Y. Nojiri and E. Takamori, *Chem. Commun.*, 2012, **48**, 1763–1765.

120 S. Yamada and Y. Nojiri, *Chem. Commun.*, 2011, **47**, 9143–9145.

121 S. Yamada and C. Kawamura, *Org. Lett.*, 2012, **14**, 1572–1575.